Simplified in-situ tailoring of cross-linked self-doped sulfonated polyaniline (S-PANI) membranes for nanofiltration applications

Hassan Alhweij[a,c,d], Emma Anna Carolina Emanuelsson[a,b], Salman Shahid[a,b,c*], Jannis Wenk[a,c*]
[a] Department of Chemical Engineering, University of Bath, Bath BA2 7AY, United Kingdom
[b] Centre for Advanced Separations Engineering, University of Bath, Bath BA2 7AY, United Kingdom
[c] Water Innovation and Research Centre (WIRC@Bath), University of Bath, Bath, BA2 7AY, United Kingdom
[d] Stantec UK Limited, Dominion House, Warrington, WA3 6GD, United Kingdom
* Corresponding authors
Jannis Wenk: j.h.wenk@bath.ac.uk
Salman Shahid: s.shahid@bath.ac.uk

Abstract

Sulfonated polyaniline (S-PANI) membranes could have wide-ranging applications due to their electrical tunability, antifouling behaviour and chlorine resistance. However, S-PANI membranes below the ultrafiltration (UF) separation range have not been successfully established. This study presents a scalable approach to produce the first in-situ cross-linked S-PANI membranes at nanofiltration (NF) range. S-PANI membranes were produced by non-solvent induced phase separation (NIPS). The presence of sulfonic groups as polymer cross-linking anchors and controlling the coagulation bath's acidic strength resulted in instant stabilisation of the selective layer, which hindered the solvent/non-solvent exchange rate. This enabled the production of a tailored membrane morphology with a dense skin layer, suppressed macro-voids, reduced porosity, enhanced tensile strength, increased hydrophilicity and solvent stability. S-PANI membranes cast in 3M HCl(aq) with MWCO≈680 g mol^{-1} (sucrose octa-acetate) showed a rejection of 99% for PEG 1000 g mol^{-1} and 91-100% for dye solution (MW range of 320-1017 g mol^{-1}) compared to 34% and 74-85% rejection for a commercial fluoropolymer membrane (nominal MWCO 1000 g mol^{-1}), respectively. The reported approach is simple and can be applied to design new classes of cross-linked solvent stable S-PANI NF membranes.

Keywords: sulfonated polyaniline, cross-linked, nanofiltration, coagulation bath, acidity

1. Introduction

Membrane separation processes are important in numerous industrial applications [1]. Nanofiltration (NF) membranes have been employed in seawater desalination pre-treatment [2], drinking and wastewater treatment [3] and food processing [4]. NF membranes cover a transition region between reverse osmosis (RO) and ultrafiltration (UF) and have a pore size of 1-5 nm with a molecular weight cut off (MWCO) of 200-1000 g mol^{-1} [5]. Separation by NF membranes is based on three primary mechanisms: size exclusion (sieving), charge interaction (Donnan exclusion effect), and solute-membrane affinity (e.g., hydrophobic attraction, hydrogen bonding) [6,7]. Polymeric membranes are preferred over other materials due to their low cost and processability [8].

Non-solvent induced phase separation (NIPS) is a commonly-used process for producing polymeric membranes with desired morphologies [9]. During NIPS, the membrane material gradually separates from a liquid polymer casting solution by phase inversion in a coagulation bath consisting of a non-solvent, typically water [10]. Phase inversion provides a gradual membrane morphology transitioning from a relative dense selective upper layer to a fully porous bottom structure with large macro-voids [11]. Altering the composition of the coagulation bath can result in simultaneous cross-linking and coagulation [12], while the presence of cross-linkable groups in the chain end or the side-chains of the polymer backbone unit is essential [13]. This eliminates need for additional solvent-based post-treatment for chemically and thermally stable membranes. The cross-linking of polymer chains within a three-dimensional network is the most common way to improve mechanical strength, solvent resistance, and permeate selectivity, while choosing an appropriate cross-linker for a particular polymer may not be straightforward [14].

Both casting solution composition and choice of solvent/non-solvent coagulation bath couples control demixing (instantaneous or delayed) and membrane characteristics, such as morphology, that in turn determine mechanical strength, permeance, rejection and fouling behaviour [14,15]. Cross-linking often diminishes the gap space between the polymer chain segments resulting in limited vibrational freedom [13]. Instant cross-linking may lead to the formation of a dense selective layer which affects the coagulation kinetics by hindering the exchange rate of the solvent/non-solvent. Delayed demixing may

be preferred to produce membranes at the NF range, because it results in a dense top layer with sponge-like substructures while inhibiting the formation of large macro-voids [17]. Contrarily, instantaneous demixing leads to a porous top layer and a finger-like substructure [18].

Polyaniline (PANI) has been explored as a free-standing polymer and blending agent to enhance membrane performance by increasing membrane hydrophilicity [19–22]. Sulfonation of aromatic polymeric membranes increases proton conductivity, mechanical strength, thermal stability, and chemical stability as compared to non-sulfonated polymeric membranes [23]. Integration of covalently-bound sulfonic ($-SO_3$) groups into a PANI backbone creates sulfonated polyaniline (S-PANI) [24], which was found to improve both antifouling behaviour [25]. S-PANI membranes showed improved chlorine resistance (250 ppm sodium hypochlorite for 3 days under different pH conditions) including a stable performance and solute rejection. In contrast, PANI membranes suffered critical structural damage with complete leakage upon chlorine exposure at the same testing conditions [26].

The production of PANI membranes in the NF range is costly, laborious and complex, requiring post-treatment cross-linking procedures with organic compounds [27–29]. Little work has been done on NF S-PANI membranes, while recent efforts to condition S-PANI membranes resulted in tight UF membranes (1,800 g mol^{-1} MWCO) [25] with improved solvent stability but low permeance. Developing simple methods for producing cross-linked and solvent stable S-PANI membranes in the NF range is critical for unlocking their full application potential.

Exposing the S-PANI casting solution to a high strength acidic coagulation bath could yield cross-linked membranes in the NF range, due to: (a) associated acid doping with cross-linking [27], (b) interaction between sulfonic and amine groups [30], (c) pH effects on polymer re-assembly [31], and, (d) delayed demixing. In this work, simultaneous in-situ cross-linking and coagulation of S-PANI membranes in a high acidity solution to produce membranes at the NF range was systematically investigated for the first time. The proposed procedure is simple, fast, and cost-efficient.

S-PANI powder was synthesised by free-radical polymerisation. The membrane cast solution was prepared and applied over a non-woven support layer. Membranes were produced by NIPS in pure water, 1M and 3M HCl aqueous coagulation baths, respectively. The polymer molecular weight was identified by gel permeation chromatography (GPC). Sulfonation of PANI polymer was determined

using energy dispersive X-ray (EDX) analysis. Membrane properties were analysed by Fourier transform infrared spectroscopy (FT-IR), X-ray photoelectron spectroscopy (XPS), X-ray diffractometry (XRD), scanning electron microscopy (SEM), gas adsorption-desorption, mechanical analysis, thermal analysis such as thermogravimetric analysis (TGA) and differential scanning calorimetry (DSC), contact angle (CA) and membrane surface charge measurements. Cross-linking is hypothesized to occur at the polymer doping sites (imine and sulfonic groups) and the change in ion exchange capacity was measured by titration. Membrane water uptake, hydrolytic stability and dimensional stability were verified after wetting at different water bath temperatures. Alkaline stability was also confirmed by measuring the weight loss after wetting the membrane in basic aqueous solution. The polymer re-assembly process (precipitation) was explored by transmission electron microscopy (TEM). Precipitation kinetics were determined by measuring the solvent/non-solvent demixing rate [32]. Solvent stability in static condition, swelling degree and gel content were also quantified. Membrane permeance and rejection performances were determined via filtration experiments. Permeance and rejection benchmarking were conducted with a commercial membrane of nominal MWCO 1000 g mol^{-1}.

2.Experimental

2.1. Materials

Chemicals were obtained from various commercial suppliers and used as received. A list of chemicals is provided in the supporting information (SI), Materials S1. All solutions were prepared with deionised (DI) water produced from an ELGA deioniser (PURELAB Option).

2.2. Synthesis of S-PANI polymer

Established methods for sulfonation of aniline monomer before polymerisation (pre-sulfonation) for S-PANI synthesis are described elsewhere [25,33]. Here, a modified S-PANI polymer synthesis was used. A detailed description of the synthesis is provided in SI, S-PANI synthesis S2. In brief, ammonium persulfate aqueous solution was added dropwise to a glass beaker surrounded by ice containing aniline,

metanilic acid (1:1 molar ratio) and hydrochloric acid solution (1M) within controlled time intervals for a prolonged time i.e., 13 h. The resulting S-PANI salt precipitate at 72±1% yield was filtered, washed, dried, sieved in 160 µm and stored until required.

Gel permeation chromatography (GPC) was used to characterise the dried S-PANI powder to identify the weight average and the degree of polymerization dispersity. A detailed description of the molecular weight measurement is provided in SI, Polymer molecular weight determination S3. The average MW was calculated as 46,898 g mol^{-1} with a polydispersity of 1.93. The incorporation of the sulfonic groups to the polymer backbone and the degree of sulfonation of the S-PANI powder was confirmed by SEM-EDX (details provided in SI, Energy dispersive X-ray S4). The calculated sulfur to nitrogen (S:N) ratio of the synthesised S-PANI is 0.43 (SI, Table S1) corresponding to a fully doped S-PANI [25].

2.3. Membrane fabrication

A detailed description of the membrane fabrication is provided in SI, Membrane fabrication S5. In brief, S-PANI membranes were prepared by the NIPS method. The solution (20 wt% SPANI) was used to cast 200 µm membranes (clearance gap) at room temperature at a controlled relative humidity of ~30%. Membranes formed after immersion precipitation in the coagulation bath solution at room temperature, considering a consistent evaporation time of 10 seconds before immersing the cast film into the coagulation bath. An overview of sample nomenclature and the conditions applied is provided in Table. 1.

Table. 1 In-situ and post-treatment conditions of the tested S-PANI membranes.

Membrane	Membrane type	Coagulation solution	Post-treatment
M1	S-PANI	Pure water	-
M2	S-PANI	1M HCl	Stored in pure water for a week
M3	S-PANI	3M HCl	Stored in pure water for a week
M4	S-PANI	Pure water	Doped in 1M HCl overnight
M5	S-PANI	Pure water	Doped in 3M HCl overnight
M6	S-PANI	1M HCl	-
M7	S-PANI	3M HCl	-
M8	Commercial composite fluoropolymer	-	-

2.4. Membrane characterisation

A detailed description, including suppliers of analytical equipment, is provided in SI, Membrane characterisation S6. In brief, the chemical properties of S-PANI membranes were determined using an FT-IR spectrometer. The change in the chemical state of the sulfur and nitrogen atoms was analysed by X-ray photoelectron spectroscopy (XPS). The ion exchange capacity was measured using a titrator. The S-PANI membrane water uptake, hydrolytic stability and dimensional stability were verified after wetting at different water bath temperatures. Alkaline stability was also confirmed by measuring the weight loss after wetting the membrane in basic aqueous solution. The polymer structure was analysed by X-ray diffractometry (XRD). The morphological properties, such as membrane surface and cross-sectional area, including the change in the thickness of the selective layer of the membranes, were investigated by SEM. The S-PANI re-assembly process in neutral and acid aqueous solution was investigated by transmission electron microscopy (TEM). The change in membrane porosity was measured by N_2 adsorption-desorption. To understand the effect of the simultaneous cross-linking which resulted in the formation of the dense selective layer, precipitation kinetics were investigated by measuring the change of relative concentration of total organic carbon (TOC) in the coagulation solution at time (t) and at infinite time (∞) defined here as 24 h immersion. Thermal and mechanical analysis was carried out to explore the effect of the cross-linking. Solvent stability was determined by soaking the membranes for two weeks in *N,N*-dimethylformamide (DMF). In parallel, PANI membranes were produced at the same conditions as S-PANI for comparing the role of the sulfonic groups in the cross-linking process. The swelling degree and the gel content were measured using different polar protic, polar aprotic and nonpolar solvents.

The hydrophilicity of the membranes was measured by sessile dynamic droplet penetration using a contact angle goniometer. Membrane filtration experiments were conducted in dead-end mode with a magnetic stirrer. To ensure that all H^+ ions were leached out during the prolonged rinsing process, the pH measurements of permeates at different filtration stages were conducted and reported as an average of three samples. The solute rejection was carried out using different solutions containing dyes, PEG

(1000 g mol^{-1}) and sugar. The membrane surface charge and dye feed solutions' zeta potential were measured to understand the charge interactions between membranes and dye solutes.

2. Results and Discussion

FT-IR spectroscopy, XPS and XRD analysis

Fig. 1 shows the FT-IR spectra of M1-M3. Characteristic transmittance bands of the S-PANI were observed at 1595 cm^{-1} (quinoid C = C stretching), 1497 cm^{-1} (benzenoid C = C stretching) [25]. The presence of aromatic amine C − N stretching was observed at 1295 cm^{-1} for all samples. C − C bending for all samples was distinct at 816 cm^{-1} [34,35], and symmetric S = O stretching was detected at 1033 cm^{-1} and 708 cm^{-1} [36,37]. Results indicate the introduction of sulfonate groups to PANI structure in agreement with the literature [38]. Nonetheless, M2-M3 exhibited a peak shift from 1168 cm^{-1} (M1) towards 1148 cm^{-1}. The original peak was assigned to a strong asymmetric stretching vibration of S=O (sulfonate) whereas the new detected peak was linked to S=O stretching of sulfonamide bonds [39]. Similar peak shifts were reported for sulfonamide formation [40–42].

The relative intensity changes of the transmittance band at 1033 cm^{-1}, which is assigned to the stretch vibration of the sulfonic acid group, decreased after cross-linking. This could be attributed to the partial consumption of the sulfonic acid groups (due to the formation of sulfonamide groups) during the cross-linking process. The aromatic imine C = N stretching at transmittance band 1111 cm^{-1} [29] was only noticed for M1 and disappeared for M2-M3. The imine nitrogen double bond may break on either side of the quinoid ring reacting with the sulfonic group during the polymer re-assembly process. This would lead to an increased benzoid to quinoid ring ratio which then prevents re-dissolution or dispersion when exposed to aprotic solvents [43]. The pronounced changes in the FT-IR spectra of the M2-M3 samples compared with M1 indicate a potential interaction between sulfonic groups and nitrogen within S-PANI during the polymer re-assembly process.

The cross-linking reaction may involve nucleophilic Sn1 substitution between an electron pair donor (secondary amine) and an electron pair acceptor (sulfonic group). Also, reactions occur between NMP/4MP solvents and HCl(aq) in the coagulation bath as reported elsewhere [44]. These reactions

involve degradation of NMP potentially impacting polymer precipitation during re-assembly and the polymer-polymer bonding.

Cross-linking of M2-M3 takes place during the membrane solidification rather than after. The liquid state of the polymer solution makes the polymer chains more accessible and susceptible for reaction i.e., potential nucleophilic Sn1 substitution or due to the side reaction between the NMP/4MP solvents and the HCl(aq), enabling a higher degree of cross-linking of the entire bulk of the membrane. Exploiting the enhanced reactivity of liquid state aromatic polymer solutions for in-situ cross-linking has been previously reported [12]. Post-treatment of S-PANI membranes in their solid-state in acidic solution, conducted with M4-M5, does not interfere with the sulfonic groups because of the absence of polymer mobility. The effect of soaking solidified S-PANI membrane in acidic solution is limited to the introduction or withdrawal of protons at polymer doping sites, as illustrated in SI Fig. S15.

Cross-linking of PANI membranes in solid-state requires an organic solvent to swell the polymer and allow contact between the polymer chains and the introduced cross-linker [27]. Alternatively, a heat source could be employed in the presence of the cross-linker to facilitate cross-linking during the condensation process [29].

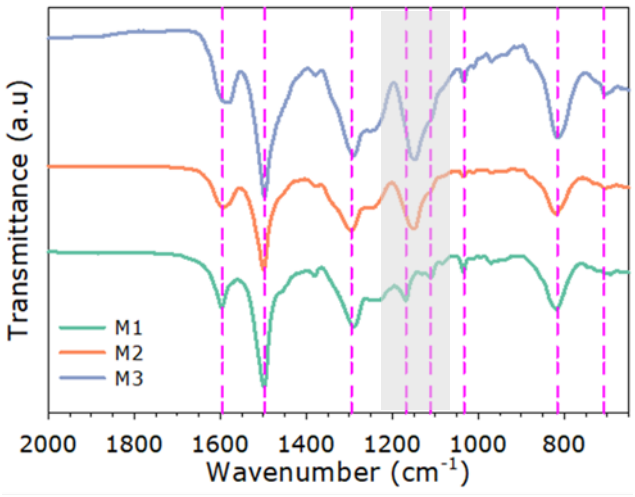

Fig. 1 FT-IR spectra of membranes produced in neutral coagulation bath (M1) and acidic coagulation bath (M2-M3).

High-resolution XPS was also used to study M1-M3. The core-level spectra of carbon (C 1s) for all membranes M1-M3 was aligned confirming calibration (XPS spectra S8, Fig. S16a), while oxygen peaks were similar (Fig. S16b). Core level spectra of sulfur S 2p of M1 were higher compared to M2 and M3 suggesting an increased oxidation state or effective nuclear pull in M1 (Fig. S16c). Slight

change in core level spectra N 1s was observed between M1 and M2-M3 (Fig. S16d). Both XPS and FT-IR results are in agreement suggesting a change in the chemical state of the sulfur and nitrogen bonding following the cross-linking reaction.

XRD was used to investigate changes in polymer crystal structures of M1-M3. PANI and its derivatives have semi-crystalline structures showing three different XRD peaks [45]. Fig. 2 provides XRD of M1 with three peaks at 2Θ=18.4°, 27° and 42°, as expected. M2 and M3 exhibited two distinctive peaks at 2Θ=24° and 40.4°. M2-M3 showed a broader peak at 2Θ=40.4° compared to M1 while the peak at 2Θ=18.4° disappeared. This suggests that cross-linking of M2 and M3 was less structured than M1 which can be ascribed to shrinkage of the intersegmental distance of polymer chains [25].

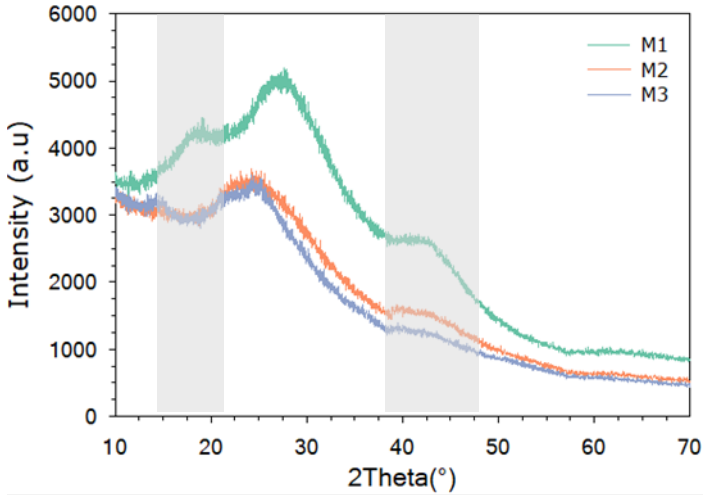

Fig. 2 XRD patterns of S-PANI membranes M1-M3.

Ion exchange capacity and water stability

The presence of amine/imine groups and sulfonic cation-exchange functional groups makes the S-PANI a promising material for fuel cell applications [46,47]. Therefore, changes in the chemical state of the ion exchange functional groups are expected to influence the ion exchange capacity. The ion exchange capacity (IEC) of M1 and M2-M3 was measured via titration. A significant reduction of about 86% in the IEC was observed for M2 compared to M1, while a marginal difference was noticed between the cross-linked membranes M2 and M3 (Table 2). The change in the IEC could be attributed to the consumption of the amine/imine groups and cation-exchanging sulfonic groups.

Water uptake measurements showed that cross-linking caused about 20 to 24% suppression of uptake for M2-M3, respectively, compared to M1. The lower water uptake could be attributed to the three-dimensional network of the cross-linked membranes.

Table. 2 Ion exchange capacity (IEC) and water uptake of S-PANI membranes M1-M3.

Membrane	IEC (meq g^{-1})	Water uptake
M1	1.29±0.2	1.94±0.14
M2	0.18±0.03	1.55±0.04
M3	0.16±0.03	1.47±0.03

The water stability test was performed by immersing membrane samples in pure water at 20, 40 and 80°C for 4 h while the dry weight was measured before and after the test. All the tested membranes M1-M3 showed a stable and consistent dry weight as shown in SI, Table S2. Also, the UV absorbance spectra of the water bath did not show an indication of leaching impurities from the membrane samples. M1-M3 exhibited dimensional stability in a pure water bath at different temperatures 20, 40 and 80°C overnight. Similarly, M1-M3 exhibited dry weight stability before and after soaking in 0.1 NaOH(aq) for 24 h at 20°C. The resulting membranes were alkaline stable, insoluble, and their dimensions were stable even at 80°C deionized water.

Morphology and porosity

Fig. 3a-c shows SEM surface images of membranes M1-M3. High magnification SEM images provide no apparent difference between the surface morphologies of different S-PANI membrane samples. This demonstrates that the acidic strength of the coagulation solution and the doping/dedoping process of the S-PANI membranes does not have a noticeable effect on the surface morphology. Fig. 3d-f shows SEM images of cross-sectional areas of membranes M1-M3. All membranes exhibited a typical asymmetric morphology of phase inversion, including a dense skin layer, a transition region and a porous bottom layer [10,48]. Membranes prepared in acidic coagulation solution (M2-M3) had a denser skin layer with suppressed macro-void structure (Fig. 3e-f) compared to membranes produced in pure water (M1, Fig. 3d). The in-situ cross-linking of the polymer matrix resulted in the formation of a dense skin layer which hindered the demixing rate of solvent/non-solvent and inhibited the formation of large macro-voids. Membranes with dense substructure are favoured over finger-like structures due to the enhanced solute rejection and improved mechanical strength [9,49,50]. The doped sample of the cross-linked membrane

(M6-M7) exhibited identical morphological structure to the dedoped samples M2-M3 as shown in the SI, Morphology S10 Fig. S17c-d. Post-treatment doping of M4 and M5 with H^+ ions (SI, Morphology S10 Fig. S17a-b) resulted in similar structures compared to the pristine M1 membrane (Fig. 3d), in agreement with a previous study [20]. Morphological differences were more obvious for the cross-linked membranes while leaching of residual H^+ ions did not induce an apparent change of membrane structure.

The morphological changes were quantified by measuring the thickness of the selective layer and the overall membrane thickness (excluding the support layer). Fig 4d-f shows an increase of selective layer thickness from 737 nm to 794 and 1700 nm for M1, M2 and M3, respectively. The overall membrane thickness decreased gradually from 94.8 µm to 66.2 and 47.7 µm for M1, M2 and M3, respectively, due to increasing inhibition of macro-void formation.

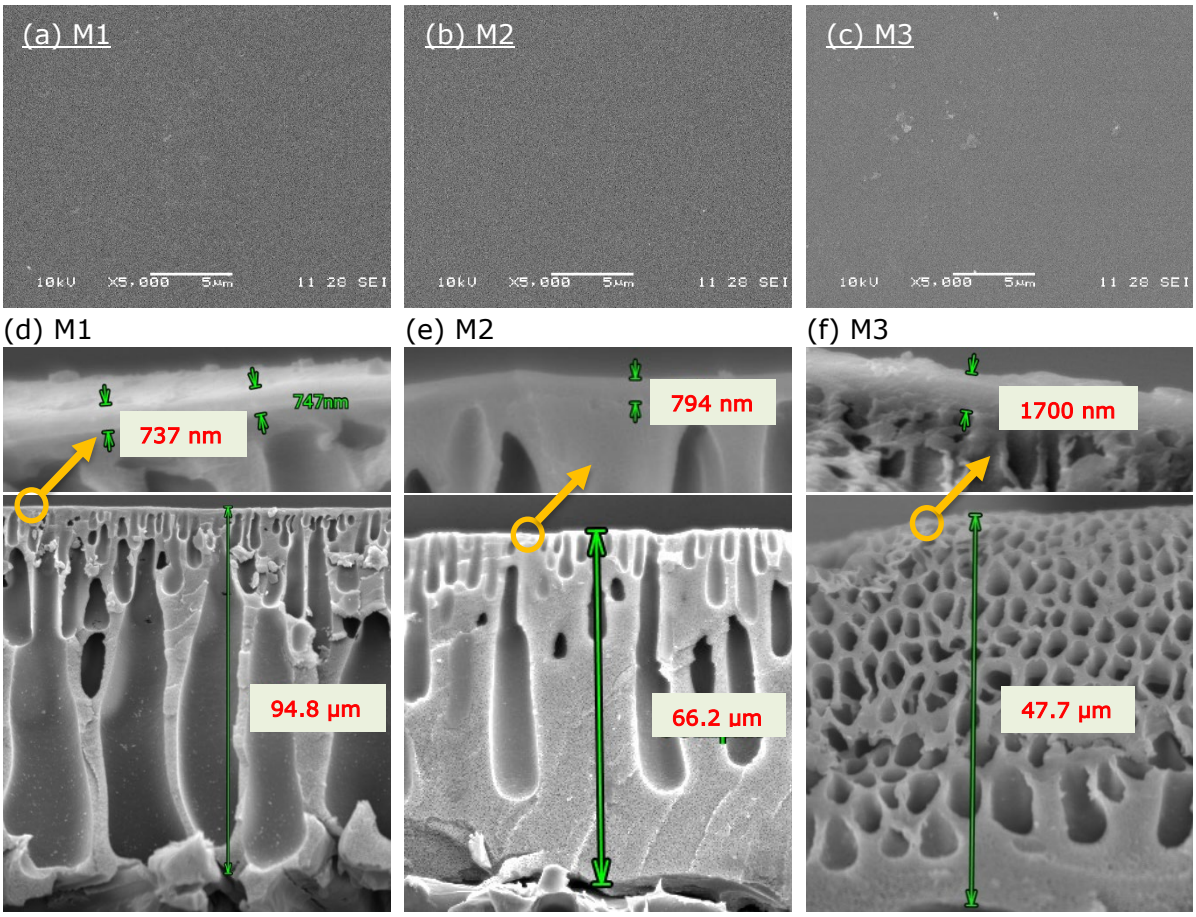

Fig. 3 SEM surface and cross-sectional area images of S-PANI membranes prepared in neutral coagulation bath (M1), 1M HCl acidic coagulation bath (M2) and 3M HCl acidic coagulation bath (M3).

To better understand the polymer re-assembly (precipitation) process, 2 mL of S-PANI polymer solution (0.2 wt/wt%) was added to 18 mL of neutral and acidic coagulation bath. The visual observation and TEM images showed different precipitation structures. Immersing the polymer solution in an acidic coagulation bath formed an organised flaky structure whereas the precipitated polymer in a neutral coagulation bath showed a cloudier solution with a fine pin floc-like structure (Fig. 4a-c). This was verified by TEM images showing a loose structure of precipitated polymer particles compared to a dense and inter-linked structure in an acidic coagulation bath (Fig. 4d-f).

PANI exhibits a different conformation in low pH coagulation solutions including forming cross-linked networks with fibrillar structure [51]. The morphology changes were attributed to the absence of H-bond interaction between the solvent and the polymer chains due to protonation of the latter. Instead, strong intrinsic interaction between polymer chains causes cross-linkages to form during the polymer re-assembly [31]. Here, the presence of sulfonic groups in S-PANI is believed to significantly affect the polymer re-assembly process and the cross-linking of the polymer matrix due to the potential interaction between the sulfonic groups the nitrogen atom in the doping sites. A solvent stability test of S-PANI and PANI membranes formed in an acidic coagulation is reported in a separate section below to validate this claim.

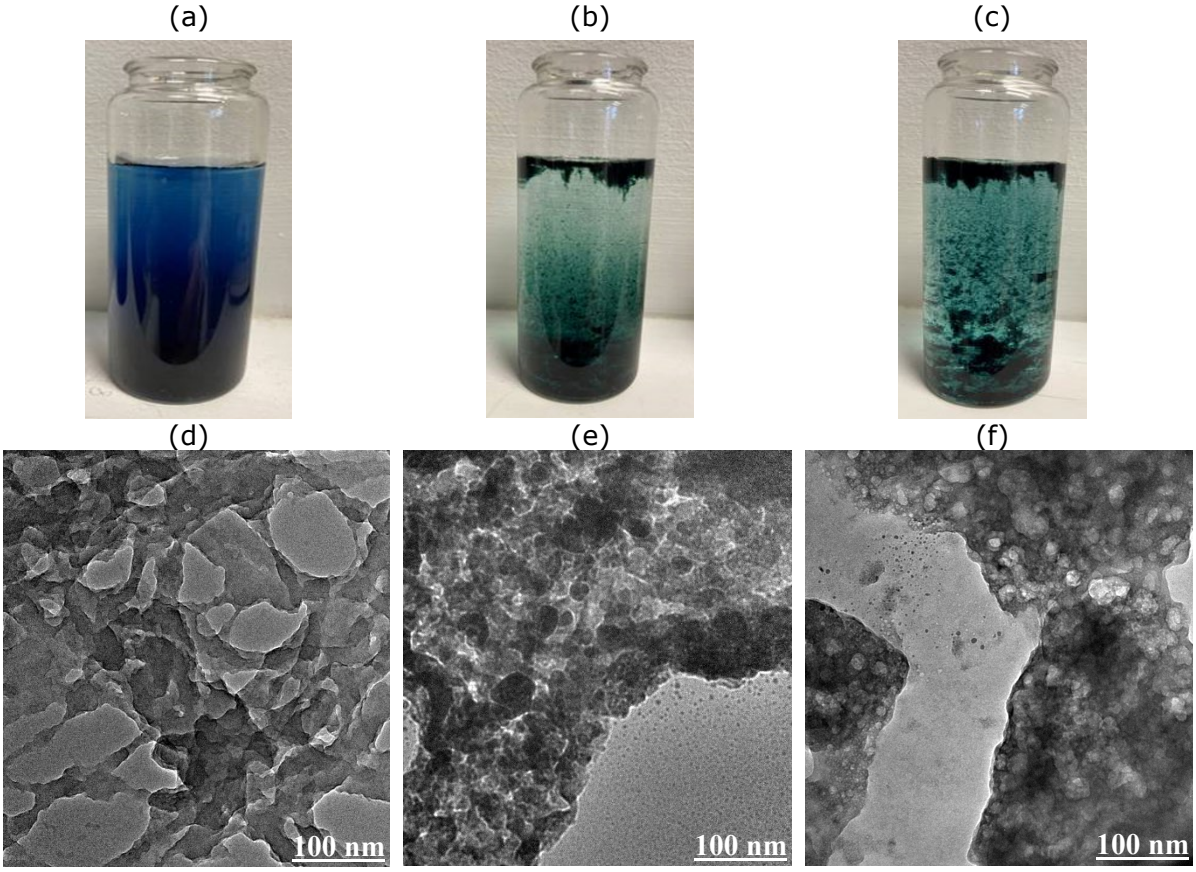

Fig. 4 Visual and TEM images of the S-PANI polymer solution in neutral coagulation bath (a, d), 1M coagulation bath (b, e) and 3M coagulation bath (c, f).

The isotherms of the porosity measurements showed a sharp decrease in the surface area of M2 and M3 (37% and 27% of M1 BET surface area, Table. 3). The change was also observed for total volume and a total area of pores <=5 nm. The maximum pore volume of M2 and M3 was 26% and 18% of M1, respectively, which corresponds to the observed suppression of the membrane's macro-voids as illustrated in the SEM images.

Table. 3 Porosity measurements of S-PANI membranes M1-M3.

	Unit	M1	M2	M3
BET surface area	$m^2\ g^{-1}$	33.6	12.5	8.9
Volume in pores <=5 nm	$cm^3\ g^{-1}$	8.83E-02	2.41E-02	1.98E-02
Maximum pore volume*	$cm^3\ g^{-1}$	1.50E-02	5.76E-03	3.68E-03
Area in pores <=5 nm	$m^2\ g^{-1}$	33.6	8.7	6.2

*At P/Po = 0.144111684

Demixing kinetics

The demixing rate was measured for the M1-M3 membrane sample as shown in Fig. 5. M1 exhibited an abrupt shift in organic solvent concentration within the first hour of polymer precipitation.

Subsequently, the concentration stabilised, showing a steady-state profile within 2 h of immersion. The instant demixing explains the formation of the finger-like voids as shown in the SEM images of membrane cross-sections. (Fig. 3d) [48]. In contrast, the in-situ cross-linking resulted in a dense selective layer which simultaneously delayed the demixing of the solvent/non-solvent, leading to a gradual release of the organic solvent to the coagulation bath over time. Note that, demixing kinetics for polymer precipitation was obtained by measuring the solvent leaching rate into the coagulation solution [32,52–54]. Light transmittance or microscopy techniques determining demixing kinetics [55–57] could not be employed due to the dark green colour of S-PANI.

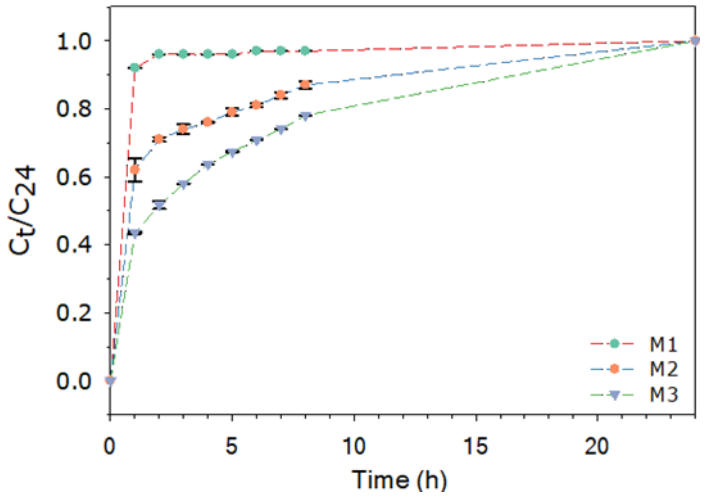

Fig. 5 S-PANI solvent demixing kinetics in neutral (M1) and increasingly acidic (M2, 1M HCl; M3, 3M HCl) coagulation solutions.

Thermal and mechanical analysis

Fig. 6 shows the TGA results which elucidate the change of weight during controlled heating as a percentage of the initial membrane sample weight and the derivative weight with respect to temperature up to 600°C. Plotting the derivative weight loss showed a first peak in the range of 20–120°C for the pristine M1 (~2.6%) and extended further to 160°C for the cross-linked M2-M3 membrane samples (~12-15%). This was attributed to the evaporation of entrapped water molecules in the polymer matrix and any residual 4-methylpyridine (4MP). The second weight-loss peak of the M1 sample was in the range of 390-590°C. The cross-linked membranes showed different thermal degradation behaviour in the range of 340-410°C for the M2 membrane, followed by the integrated broad and less intense peak to 590°C. M2 showed a more intense reduction in weight than M3 at the second peak. The weight loss at such high-temperature band was assigned to free N-methyl-2-pyrrolidone (NMP) volatilisation and

release of NMP molecules, which are hydrogen-bonded to the amine groups of S-PANI [58]. The DSC thermograms also showed that the glass transition temperature of the M1 membrane sample was shifted down from 243°C to 204°C and 187°C for the cross-linked membranes M2 and M3, respectively (SI, Differential scanning calorimetry S12 Fig. S24-S26). PANI membranes contain considerable amounts of NMP, about 18% by weight [58]. The cross-linked membranes might have entrapped a surplus quantity of NMP compared to M1 due to the dense structure. NMP could have a plasticising effect at high temperatures resulting in lower glass temperature and a further change in the thermal behaviour.

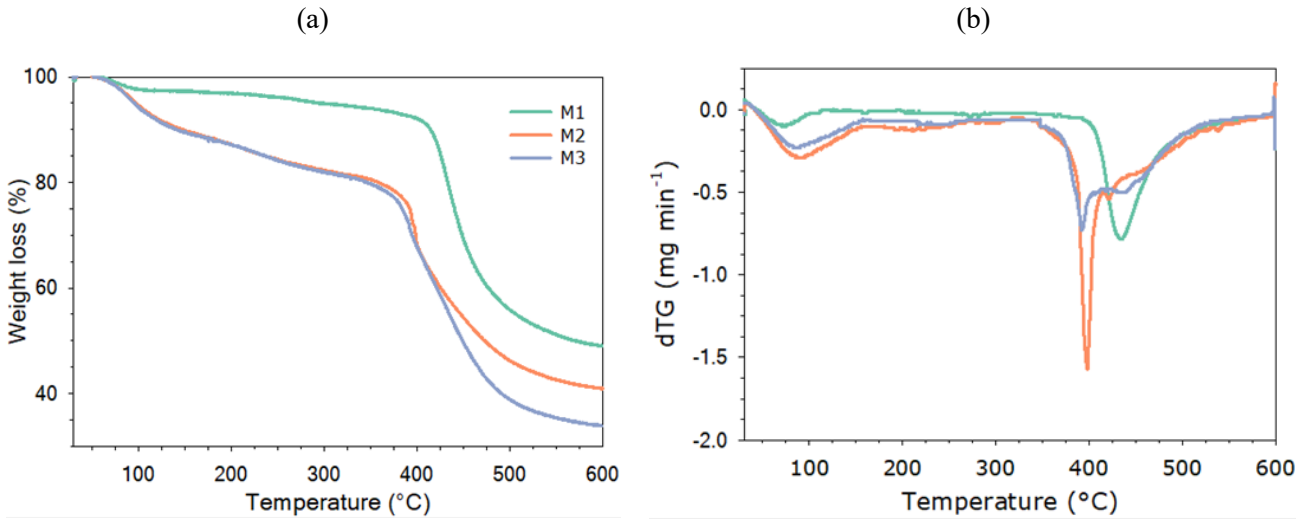

Fig. 6 TGA curves for pristine and cross-linked S-PANI membranes (a) weight loss (b) derivative weight loss with respect to temperature from room temperature to 600°C.

Fig. 7 shows the mechanical strength and the elongation at the breakage point of the S-PANI membranes, M1-M3 at room temperature. The mechanical strength of the cross-linked membranes M2-M3 is 2.3 times higher than the pristine S-PANI membrane M1, whereas a slight and inconsistent change in the elongation at breakage was observed for all samples. The cross-linked polymer structure exhibits a dense three-dimensional network, with limited freedom for motion by the individual segments of the molecules' steric hindrance to chain movement, which enhanced the mechanical strength.

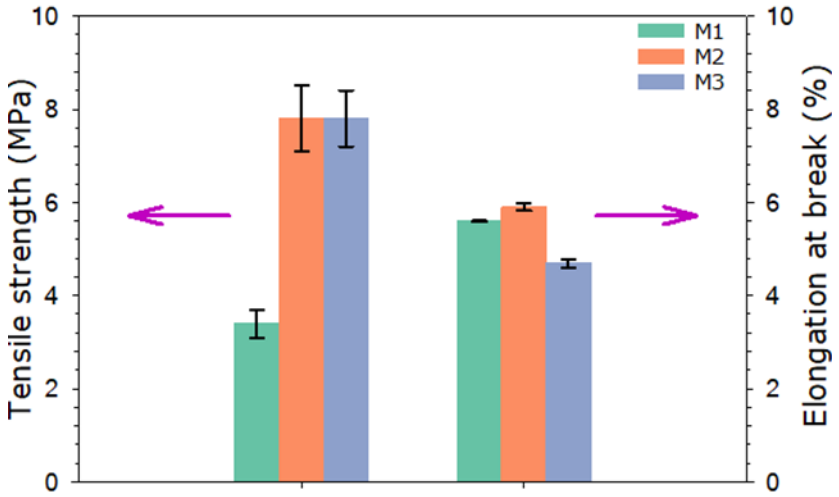

Fig. 7 Mechanical properties of the pristine M1 and cross-linked (M2-M3) S-PANI membranes.

The commercial membrane was cast over a support layer which dominates the membrane's tensile strength. As such, the tensile strength of the free-standing S-PANI membrane and commercial membrane values are not comparable.

Solvent stability

Solvent stability in DMF as an exemplary solvent was tested. Fig. 8 shows the effect of DMF on membranes stability after immersion for two weeks. M1 readily dissolved resulting in a vivid blue solution. M2 and M3 were resistant to DMF showing only a slightly discolouring of the solution after 30 minutes without any subsequent changes over the observation time of two weeks. Contrastingly, PANI membranes formed in a pure water and acidic coagulation bath (M1', M2', M3) dissolved in DMF (Fig. 8b). M2' and M3' were more resistant than M1', while all samples dissolved within one hour. Solvent stability of M2 and M3 may be attributed to the formation of interchain bonds, making the material less vulnerable to solvent attack.

Fig. 8 Effect of DMF on membrane stability after two weeks.

340 Mass swelling degree and gel content

341 Identifying the extent of swelling for polymeric membranes is essential to understand their transport
342 properties and behaviour while being exposed to organic solvents [59]. A set of organic solvents
343 including Methanol (MeOH), Isopropanol (IPA), Acetone (AC), Toluene (TOL), Tetrahydrofuran (THF)
344 was used to determine the membrane swelling (Fig. 9a) and solvent stability (Fig. 9b). The mass
345 swelling degree of M1 increased in the sequence of TOL<MeOH<AC<IPA<THF. The maximum
346 swelling was found for THF at 88±8%. M1 did not qualify for swelling tests with DMF due to instant
347 dissolution. Swelling trends for M2-M3 were different and in the order AC<THF<MeOH<IPA≈TOL.
348 The difference in the swelling degree trend between M1 and M2-M3 could be attributed to the change
349 in the Hansen solubility parameter following the cross-linking reaction. Generally, significant polymer
350 swelling with strong polymer-solvent interaction is anticipated for polymers that have similar Hansen
351 solubility parameters to the surrounding solvent [60]. The highest swelling degree for M2 was about
352 9±1% (TOL≈IPA) while the THF swelling was only 3±0.2%. Marginal difference in the swelling degree
353 was observed between M2 and M3. The decreased swelling degree of M2-M3 could be explained by
354 the reduced porosity due to the inter-linked segments of the polymer. Besides, the top layer of M2-M3
355 was more hydrophilic than M1 (see also contact angle section), which effectively prevented the
356 dissolution and permeation of organic solvents into the bulk of cross-linked S-PANI matrix.

357 Fig. 9b showed membrane stability static test in organic solvents including DMF over two weeks. M1
358 was unstable in THF and DMF as the transparent solvent turned blue due to the gradual dissolution of
359 the polymer in THF while being readily dissolved in DMF. The dry mass of the M1 was reduced by
360 10±5.6% and 78.5±3.2% with THF and DMF, respectively. M1 was more stable in MeOH, IPA, AC and
361 TOL than THF and DMF as there was only a slight colour change with maximum decreased mass by
362 3.5% with MeOH. M2-M3 exhibited stability for all solvents tested providing no change in solvent
363 colour after the two weeks, except a slight discolouring with the DMF in the first 30 minutes. The dry
364 mass of the soaked membrane remained constant while showing weight loss around 4.3±0.5% (M2)
365 and 0.9±1% (M3) with DMF.

366 Functionalising the PANI polymer with sulfonic groups (pre-sulfonation) was proven to be essential for
367 the in-situ cross-linking to take place in an acidic coagulation bath. This test indicates that M2 and M3

may qualify for organic solvent applications, while extended solvent stability tests are part of an ongoing study.

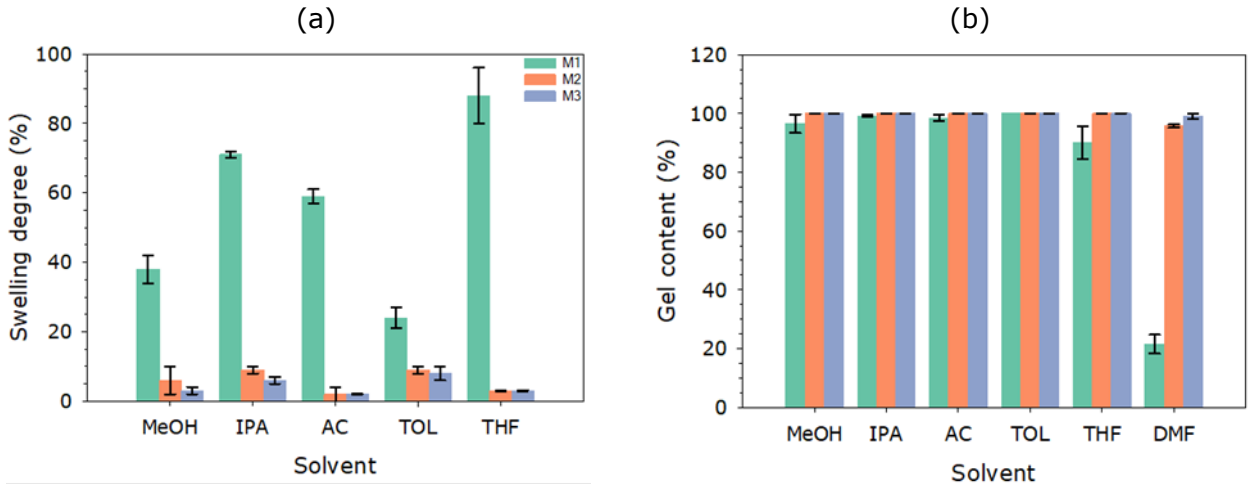

Fig. 9 Mass swelling degree and gel content of pristine and crosslinked S-PANI membranes M1-M3 in different polar protic, polar aprotic and nonpolar solvents.

Contact Angle

The hydrophilicity of the pristine and cross-linked S-PANI membranes was estimated by measuring the apparent contact angle of the membrane surface. High affinity to water with a contact angle less than 90° indicates a hydrophilic membrane. As shown in Fig. 10 the dynamic CA of M2-M3 showed a continuous and higher decline compared to M1, which provided a relatively constant value. The contact angle of M2 and M3 decreased continuously for 100 seconds. However, a slightly dynamic decrease was observed after 120 seconds, reaching a steady level (~28°) after 140 seconds. The changes in CA can be rationalised by (a) higher polarity (surface charge) of the membrane surface and therefore stronger intermolecular attraction between water and membrane surface [61–63], and, (b) the dense skin layer with less porosity produced a smoother surface which could affect the contact angle and hydrophilicity [18,48]. The hydrophilicity followed the opposite order of the contact angle: M1 < M2 < M3 with the marginal difference between M2-M3. A higher hydrophilicity with a smooth and charged surface of M2-M3 could indicate a higher antifouling property [19,29].

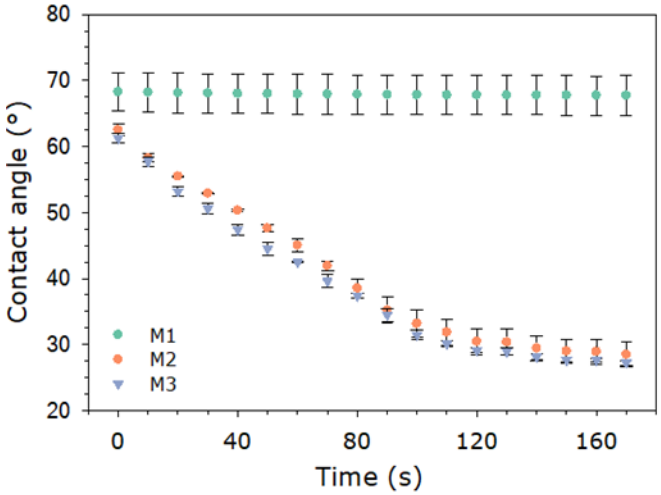

Fig. 10 The contact angle of the S-PANI membranes (M1-M3).

Membrane transport properties

The permeance of M1-M5 and the commercial M8 membranes was evaluated using three solutions: pure water (Fig. 11), PEG aqueous solution (MW 1000 g mol^{-1}) (Fig. 12a) and aqueous dye solution (MW 320 to 1017 g mol^{-1}) (Fig. 13a). The permeance of M1-M3 and M8 experienced an initial drop during the preconditioning phase due to the compaction of the membrane under the transmembrane pressure [64]. The permeance became steady (5% difference) after 30 min. A slight increase in the M4-M5 membrane permeance was observed during preconditioning and filtration, therefore, an average permeance value is shown in Fig. 11 and Fig. 12a. This can be attributed to leached H^+ ions, which increased the membrane's free volume. Soaking M4-M5 in an aqueous solution for a week with a daily change of the solution reinstated the membranes' permeance with stable and neutral permeate pH. Both residual H^+ ions on the polymer chains and the pH variability of feed solution could affect membrane permeance stability, solute rejection, and surface charge [22]. To better understand the in-filtration membrane stability and confirm the absence of residual H^+ ions in the membrane, the pH of the permeate was measured using a feed solution at neutral pH (SI, Transport properties S13 Fig. S27). Permeate pH of HCl-doped M4 and M5 decreased during filtration, indicating leaching of H^+ ions. Immersing the M4 and M5 membrane samples for a week in pure water while changing the soaking solution daily helped to de-dope the membranes and reinstate the initial transport properties with stable permeate pH. The permeate pH of M1-M3 remained stable, indicating: (a) the fabrication method of the self-doped S-PANI membrane overcame the acid leaching problem, and (b) rinsing of M2 and M3 for a prolonged time with pure water removed residual H^+ ions. The interwoven and/or double-stranded structure in the

S-PANI complex binds the acid more strongly, and thus there is no loss of sulfonated groups during the filtration, which is consistent with the literature [21,36,65]. S-PANI membranes prepared in acidic solution and left in water for one week did not show any leaching of H^+ ions that suggested stable and comparable performance in contrast to the HCl-doped S-PANI membranes that leached H^+ ions and showed unstable performance.

Fig. 11 shows that the higher acidic strength of the coagulation bath led to a considerable drop in the pure water permeance by 63-67% and 92-94%, respectively, compared to M1. Transmembrane pressure of M1, M2 and M3 increased from 2 to 3 and 6 bar, respectively, because of the change in density of the selective layer (Fig. 3) and porosity (Table. 3). The average permeance of M4 and M5 exhibited a decline of around 12-14% compared to M1. The cross-linking resulted in a decrease in the gap space between the polymer chains during the re-arrangement process, explaining the performance change of M2 and M3 [19,32,66]. Doping the S-PANI membranes in acidic solution resulted in a slight swell [61]. The proposed changes could reduce the pore size of the membrane and create further water transport resistance as illustrated in SI, Transport properties S13 Fig. S28. The increase in the doping solution's acidic strength (polymer chains swelling) with reduction of membrane permeance and increase in solute rejection quantitatively confirmed our proposed hypothesis.

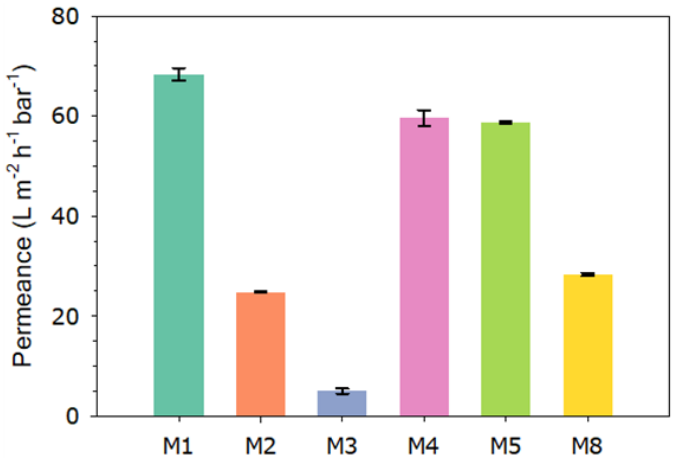

Fig. 11 Pure water permeance for the S-PANI membranes (M1-M5) and the commercial membrane (M8).

Fig. 12a and Fig. 13a show the effect of the solutes' concentration polarisation on the membrane performance. A generic permeance decline of 36-56% and 71-79% was observed for the tested

membranes with PEG solution and the dye feed solutions, respectively, compared to pure water permeance. The PEG and dye solution permeance results are in good consistency with the pure water results reflecting the effect of the coagulation bath's acidic strength. NF membranes are known to operate at transmembrane pressure around 2-10 bar with approximate pure water permeance 5-50 L m^{-2} h^{-1} bar^{-1} [48]. The obtained permeance results of M1, M2, M3 and M8 agree with the literature [67,68]. The permeance and rejection of the dye solution through the HCl-doped M4 and M5 membranes were not evaluated due to the interaction between the dye solutes with the leached H^+ ions leading to biased UV absorbance and incorrect dye rejection [69].

Fig. 12b shows that M1 to M5 and M8 produced distinct MWCO curves with the PEG rejections in the following order: M1<M8<M4<M5<M2<M3. The different PEG rejections between pristine and HCl-doped M4-M5 membranes were attributed to the contraction of the membrane pore size, because of the different free volumes in the skin layer. The strength of the HCl doping solution enhanced the PEG-1000 g mol^{-1} rejection to 40% and 49% for the M4 and M5 membranes, respectively, in comparison with 29% rejection by M1. A substantial increase in the PEG rejections to 66% and 99% were obtained by M2 and M3, respectively. The higher density of the top skin layer and the change in the membrane conformation to the suppressed macro-void structure with less porosity was directly reflecting the PEG rejections. To evaluate the enhanced performance of S-PANI membranes, the commercial M8 membrane rejection was also acquired. A rejection of around 34% was achieved at 1000 Da in comparison with nominal (labelled) MWCO around 90%. The PEG comprehends a series of water-soluble, linear chain polymers of oxyethylene units, which are mainly present as a helix [70]. The hydrated polymer shows a conformation as an expanded random coil [71], therefore, the wiggling effect of the linear PEG could contribute to the solutes carry-over to the permeate under applied pressure which explains the difference between the measured MWCO and the nominal rejection as found in previous work [72]. The wiggling effect may underestimate the actual MWCO of the tested membranes. Additionally, the measured TOC of the feed PEG solution is high (≈312 mg L^{-1}) which may also underrate the rejection of the tested membranes. To exclude the PEG wiggling effect and identify the exact MWCO of the NF membrane (M3), rejection for sucrose octa-acetate and raffinose was

455 determined at TOC feed of 20 mg L^{-1}. Table. 4 shows that the cross-linked M3 membrane has a MWCO
456 around 680 g mol^{-1} compared to 900 g mol^{-1} using the PEG1000 solute.

457 Table. 4 The MWCO determination of the NF membrane (M3) using sugar solutes.

Solute	MW (g mol^{-1})	Rejection (%)
Sucrose octa-acetate	678.6	90.0±2
Raffinose	504.4	60.0±3

458

459 The nominal MWCO of M8 (charged membrane), as presented by the supplier, might have been
460 measured based on the different dye solutions. The Donnan effect could have resulted in such higher
461 dye rejection and apparently lower MWCO. On the other hand, PEG is electrically neutral, and its
462 rejection will not be influenced by the Donnan effect, thus resulting in lower rejection of M8 for PEG
463 solution and higher MWCO [72]. The overall outcome shows coherence between the permeance and
464 the rejection results. The results also suggest that M3 was the only one to be classified as an NF
465 membrane. The specific MWCO values of the other membranes can be determined using solutes that
466 are larger than the maximum MW of 1074 g mol^{-1} used in this work.
467 To have an accurate evaluation of the membrane rejection because of the adopted modifications, the
468 rejection test of four different dyes was implemented for the M1-M3 and the commercial M8 membrane.
469 Fig. 13b shows the rejection values from 50-84% to 72-96% and 91-100% for the M1-M3 membranes
470 at a molecular weight range from 320 to 1017 g mol^{-1}. Also, M8 exhibited a high dye rejection between
471 74 to 85%. The membrane surface charge and the dye feed solution's zeta potential measurements were
472 undertaken to evaluate membrane-solute charge interaction, which could influence the dye exclusion
473 and show higher apparent rejection of dye [73]. Fig. 14a shows the surface charge of M1-M5 and the
474 commercial M8 membrane. The reported surface charge of the S-PANI membrane doped in acidic
475 solution at pH 4.5 was around 20 mV [26,74], which falls within the same range as the HCl-doped M4
476 membrane. It can be observed that the higher acidic strength enhanced the surface charge of the doped
477 M5 membrane to 25 mV. This can be attributed to the abundance of H^+ ions which protonated the
478 polymer chains and therefore implied an increase of membrane surface charge. M2 and M3 membranes
479 exhibited a significant step-change (74%) in surface charge even after leaching of all residual H^+ ions
480 compared to the M1 membrane. Compared to the S-PANI membrane, the surface charge of the M8 was

obtained (-11.7±3.4 mV) and the negative surface charge agreed with the literature values [75]. The zeta potential of the four tested dye feed solutions was measured, as shown in Fig. 14b. All dye solutions were negatively charged with zeta potential ranging from -1.6 to -27.4 mV. The difference between the S-PANI membrane surface charge and the zeta potential of the dye solutes could underestimate the membranes' rejection, in contrast with the commercial membrane, where the actual rejection rate could be overestimated.

The anionic charge of the aqueous dye feed solution and the negative surface charge of the commercial M8 membrane appeared to have a contribution to the solute repulsion leading to higher rejection due to the Donnan effect [72]. However, all tested S-PANI membranes (M1-M3) which had an opposite charge to the retained dye solutes, also demonstrated a higher rejection than the PEG solutes. To differentiate the S-PANI membrane's dye rejection mechanism, i.e., size-exclusion versus adsorption, as there would not be any Donnan exclusion in the cationic membrane for anionic molecules, the adsorbed dye mass was quantified for the M1 membrane based on the mass balance of the feed, concentrate and the permeate, (SI, Table. S3). The mass of the adsorbed dye to the M1 membrane was in the following order Indigo carmine>Rose bengal>Methylene blue. The dye mass adsorption follows similar order to the dye's zeta potential -27.4, -6.1 and -1.5 mV, respectively. The significant difference in the membrane surface charge and the Indigo carmine solution's zeta potential ($\Delta V \approx 38.9$ mV) resulted in the highest mass adsorption (≈42%) compared with the methylene blue dye solution where the adsorbed mass ≈16%. This means that the size exclusion is the dominant rejection mechanism for the methylene blue dye solutes for the S-PANI membranes. The bulky nature of the dye molecule showed a higher rejection compared to the flexible PEG molecule for the same MW of PEG and dye solution, as the PEG chain allows it to wiggle through the small size pore while the dye molecule clogs the pore [76,77].

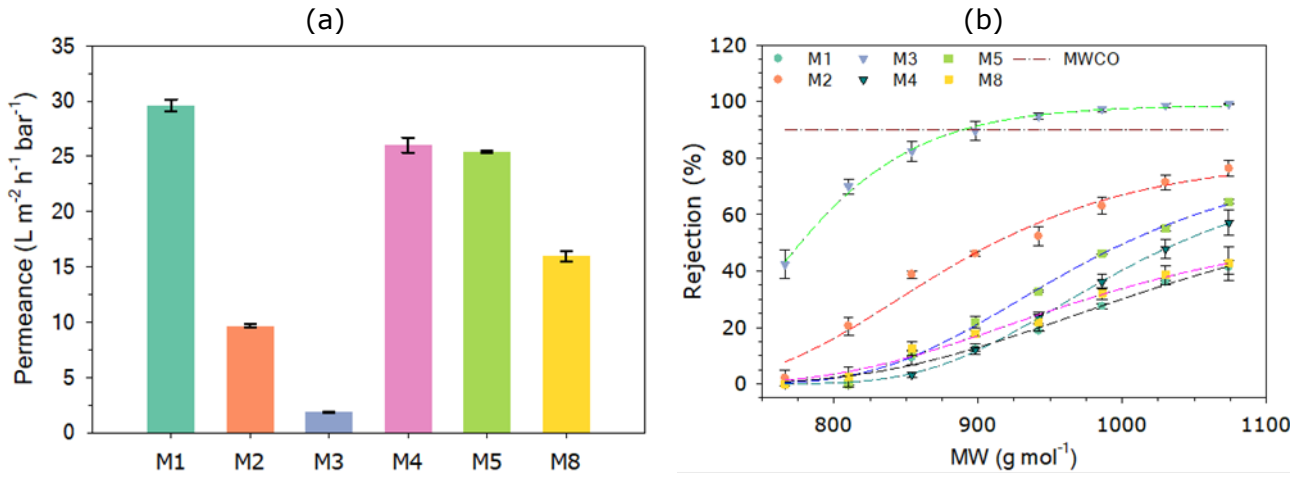

Fig. 12 (a) PEG permeance and (b) rejection of the S-PANI membranes (M1-M5) and the commercial membrane (M8).

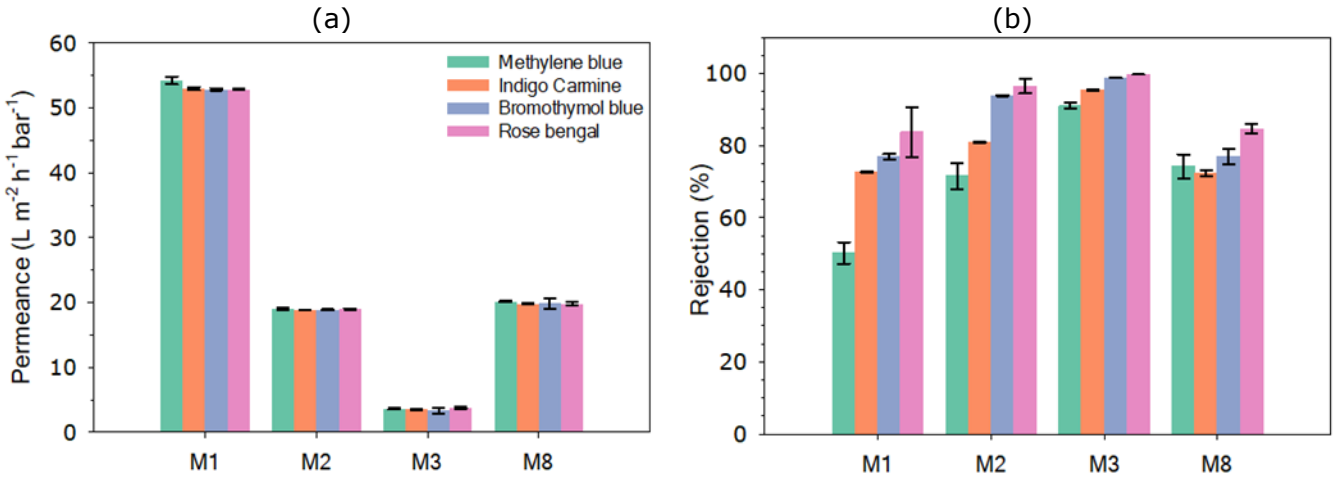

Fig. 13 (a) dye feed solution (methylene blue, indigo carmine, bromothymol blue and rose bengal) permeance and (b) rejection for of the S-PANI membranes (M1-M3) and the commercial membrane (M8).

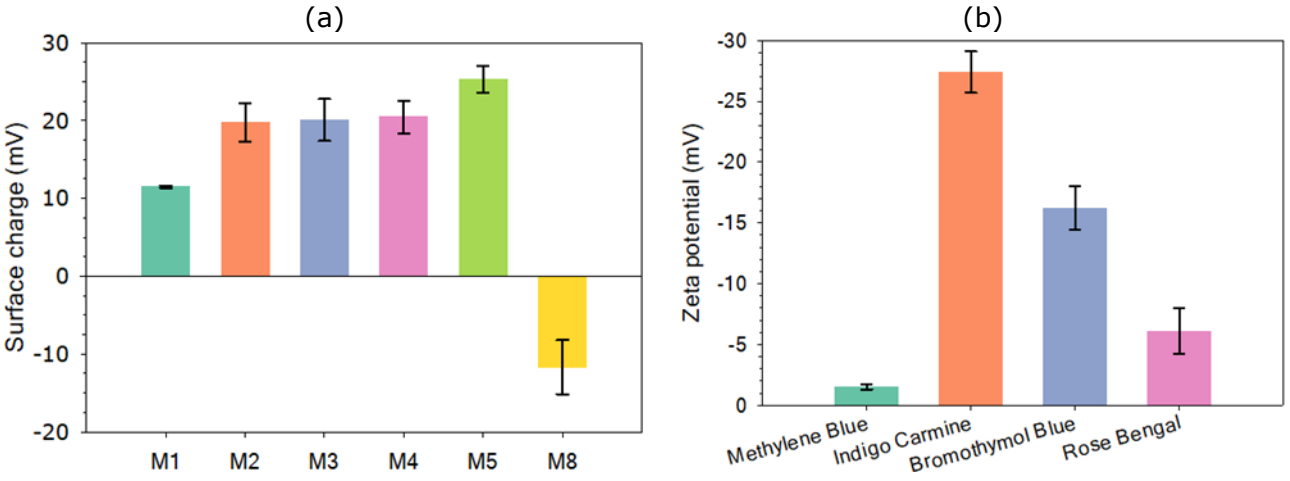

Fig. 14 (a) The surface charge of M1-M5 membranes and the commercial M8 membrane and (b) The zeta potential of dye feed solutions (methylene blue 10 mg L^{-1}, indigo carmine 10 mg L^{-1}, bromothymol blue 50 mg L^{-1} and rose bengal 10 mg L^{-1}).

4. Conclusions

S-PANI powder was synthesised by oxidation polymerisation and subsequently, integrally skinned asymmetric membranes were prepared using the NIPS technique. The presence of sulfonic groups in the polymer backbone provides the anchor to cross-link the polymer while precipitating in an acidic aqueous coagulation bath. FT-IR, XPS and XRD spectra of the SPANI membranes produced in 1M and 3M HCl(aq) coagulation bath (M2-M3) indicates a potential interaction between the sulfonic groups and the nitrogen resulting in a more amorphous matrix compared to the pristine S-PANI produced in pure water coagulation bath (M1). The reduction in the IEC for the cross-linked membranes also advocates the hypothesis of the sulfonamide formation. TEM images showed a loose structure of precipitated polymer particles in pure water, compared to a dense and inter-linked structure in an acidic coagulation bath. The simultaneous cross-linking led to an instant formation of a dense selective layer, which diminished the demixing rate. This resulted in an altered membrane conformation with suppressed macro-voids, reduced porosity, improved tensile strength, enhanced hydrophilicity, and a significant improvement in DMF solvent stability over an observation time of two weeks. The TGA of the cross-linked membranes also showed a broad and extended peak at high temperature whereas the glass transition temperature was decreased. In-situ tailored NF S-PANI membranes (M3) with MWCO≈680 g mol^{-1} (sucrose octa-acetate) showed a rejection of 99% for PEG 1000 g mol^{-1} and 91-100% for dye solutes (MW range of 320-1017 g mol^{-1}) compared to 34% and 74-85% rejection for a commercial membrane with nominal (labelled) MWCO 1000 g mol^{-1}, respectively. In summary, high-performance S-PANI membranes were prepared in-situ by exploiting cross-linkable sulfonic groups, while tailoring the coagulation bath conditions. This new simplistic, time, chemical and cost savings scalable approach can be effortlessly applied to design new classes of S-PANI membranes in NF range without the complications of using laborious post modification cross-linking methods.

5. Acknowledgements

H.A. was supported by a University of Bath research scholarship. The authors thank Matthew Jones and Simon Lewis for valuable discussion and the technicians' team at the Department of Chemical Engineering and the Bio-imaging lab at the University of Bath for support and advice. The X-ray photoelectron (XPS) data collection was performed at the EPSRC National Facility for XPS ("HarwellXPS"), operated by Cardiff University and UCL, under Contract No. PR16195.

6. References

[1] L.K. Wang, J.P. Chen, Y.-T. Hung, N.K. Shammas, eds., Membrane and Desalination Technologies, Humana Press, Totowa, NJ, 2011. https://doi.org/10.1007/978-1-59745-278-6.

[2] L. Llenas, G. Ribera, X. Martínez-Lladó, M. Rovira, J. de Pablo, Selection of nanofiltration membranes as pretreatment for scaling prevention in SWRO using real seawater, Desalin. Water Treat. 51 (2013) 930–935. https://doi.org/10.1080/19443994.2012.714578.

[3] V. Yangali-Quintanilla, S.K. Maeng, T. Fujioka, M. Kennedy, G. Amy, Proposing nanofiltration as acceptable barrier for organic contaminants in water reuse, J. Memb. Sci. 362 (2010) 334–345. https://doi.org/10.1016/j.memsci.2010.06.058.

[4] O. Akin, F. Temelli, S. Köseoğlu, Membrane Applications in Functional Foods and Nutraceuticals, Crit. Rev. Food Sci. Nutr. 52 (2012) 347–371. https://doi.org/10.1080/10408398.2010.500240.

[5] A.F. Ismail, Membrane Technology for Water and Wastewater Treatment, Energy and Environment, 2016. https://doi.org/10.1201/b19702.

[6] A.I. Schäfer, Natural Organics Removal Using Membranes Natural Organics Removal Using Membranes, CRC Press, 1999. https://doi.org/10.1201/9781420031638.

[7] P. Marchetti, M.F. Jimenez Solomon, G. Szekely, A.G. Livingston, Molecular Separation with

Organic Solvent Nanofiltration: A Critical Review, Chem. Rev. 114 (2014) 10735–10806. https://doi.org/10.1021/cr500006j.

[8] I. Koyuncu, R. Sengur, T. Turken, S. Guclu, M.E. Pasaoglu, Advances in water treatment by microfiltration, ultrafiltration, and nanofiltration, in: Adv. Membr. Technol. Water Treat., Elsevier, 2015: pp. 83–128. https://doi.org/10.1016/B978-1-78242-121-4.00003-4.

[9] G.R. Guillen, Y. Pan, M. Li, E.M.V. Hoek, Preparation and characterization of membranes formed by nonsolvent induced phase separation: A review, Ind. Eng. Chem. Res. 50 (2011) 3798–3817. https://doi.org/10.1021/ie101928r.

[10] M. Mulder, Basic Principles of Membrane Technology, Springer Netherlands, Dordrecht, 1996. https://doi.org/10.1007/978-94-009-1766-8.

[11] B. Singh, V. Kochkodan, R. Hashaikeh, N. Hilal, A review on membrane fabrication : Structure , properties and performance relationship, Desalination. 326 (2013) 77–95. https://doi.org/http://dx.doi.org/10.1016/j.desal.2013.06.016.

[12] K. Vanherck, A. Cano-Odena, G. Koeckelberghs, T. Dedroog, I. Vankelecom, A simplified diamine crosslinking method for PI nanofiltration membranes, J. Memb. Sci. 353 (2010) 135–143. https://doi.org/10.1016/j.memsci.2010.02.046.

[13] Z. Wang, Cross-Link, in: Encycl. Membr., Springer Berlin Heidelberg, Berlin, Heidelberg, 2016: pp. 479–480. https://doi.org/10.1007/978-3-662-44324-8_1809.

[14] A. Asadi Tashvigh, Y. Feng, M. Weber, C. Maletzko, T.-S. Chung, 110th Anniversary: Selection of Cross-Linkers and Cross-Linking Procedures for the Fabrication of Solvent-Resistant Nanofiltration Membranes: A Review, Ind. Eng. Chem. Res. 58 (2019) 10678–10691. https://doi.org/10.1021/acs.iecr.9b02408.

[15] A.L. Zydney, C. Ho, Effect of Membrane Morphology on System Capacity During Normal Flow Microfiltration, (2003). https://doi.org/10.1002/bit.10699.

[16] M. Elimelech, Xiaohua Zhu, A.E. Childress, Seungkwan Hong, Role of membrane surface morphology in colloidal fouling of cellulose acetate and composite aromatic polyamide reverse osmosis membranes, J. Memb. Sci. 127 (1997) 101–109. https://doi.org/10.1016/S0376-7388(96)00351-1.

[17] K. Scott, Membrane materials, preparation and characterisation, in: Handb. Ind. Membr., Elsevier, 1995: pp. 187–269. https://doi.org/10.1016/B978-185617233-2/50005-2.

[18] C.J.W. Nidal Hilal, Mohamed Khayet, Membrane Modification, CRC Press, 2016. https://doi.org/10.1201/b12160.

[19] H. Deligöz, Preparation of self-standing polyaniline-based membranes: Doping effect on the selective ion separation and reverse osmosis properties, J. Appl. Polym. Sci. 105 (2007) 2640–2645. https://doi.org/10.1002/app.26377.

[20] L.L. Xu, S. Shahid, D.A. Patterson, E.A.C. Emanuelsson, Flexible electro-responsive in-situ polymer acid doped polyaniline membranes for permeation enhancement and membrane fouling removal, J. Memb. Sci. 578 (2019) 263–272. https://doi.org/10.1016/j.memsci.2018.09.070.

[21] H. Hu, J.M. Saniger, J.G. Bañuelos, Thin films of polyaniline-polyacrylic acid composite by chemical bath deposition, Thin Solid Films. 347 (1999) 241–247. https://doi.org/10.1016/S0040-6090(99)00039-5.

[22] N.F. Razali, A.W. Mohammad, N. Hilal, Effects of polyaniline nanoparticles in polyethersulfone ultrafiltration membranes: Fouling behaviours by different types of foulant, J. Ind. Eng. Chem. 20 (2014) 3134–3140. https://doi.org/10.1016/j.jiec.2013.11.056.

[23] S.M.J. Zaidi, K.S. Lakhi, Sulfonated Block Copolymer Membrane, in: Encycl. Membr., Springer Berlin Heidelberg, Berlin, Heidelberg, 2016: pp. 1844–1845. https://doi.org/10.1007/978-3-662-44324-8_561.

[24] J. Yue, Z.H. Wang, K.R. Cromack, A.J. Epstein, A.G. MacDiarmid, Effect of sulfonic acid

group on polyaniline backbone, J. Am. Chem. Soc. 113 (1991) 2665–2671. https://doi.org/10.1021/ja00007a046.

[25] I.F. Amura, S. Shahid, A. Sarihan, J. Shen, D.A. Patterson, E.A.C. Emanuelsson, Fabrication of self-doped sulfonated polyaniline membranes with enhanced antifouling ability and improved solvent resistance, J. Memb. Sci. (2019) 117712. https://doi.org/10.1016/j.memsci.2019.117712.

[26] H. Alhweij, I. Amura, J. Wenk, E.A.C. Emanuelsson, S. Shahid, Self-doped sulfonated polyaniline ultrafiltration membranes with enhanced chlorine resistance and antifouling properties, J. Appl. Polym. Sci. (2021) 50756. https://doi.org/10.1002/app.50756.

[27] X.X. Loh, M. Sairam, A. Bismarck, J.H.G. Steinke, A.G. Livingston, K. Li, Crosslinked integrally skinned asymmetric polyaniline membranes for use in organic solvents, 326 (2009) 635–642. https://doi.org/10.1016/j.memsci.2008.10.045.

[28] M. Sairam, X. Xing, K. Li, A. Bismarck, J. Hans, G. Steinke, A. Guy, Nanoporous asymmetric polyaniline films for filtration of organic solvents, 330 (2009) 166–174. https://doi.org/10.1016/j.memsci.2008.12.067.

[29] J. Shen, S. Shahid, A. Sarihan, D.A. Patterson, E.A.C. Emanuelsson, Effect of polyacid dopants on the performance of polyaniline membranes in organic solvent nanofiltration, Sep. Purif. Technol. 204 (2018) 336–344. https://doi.org/10.1016/j.seppur.2018.04.034.

[30] V. Vijayalekshmi, D. Khastgir, Eco-friendly methanesulfonic acid and sodium salt of dodecylbenzene sulfonic acid doped cross-linked chitosan based green polymer electrolyte membranes for fuel cell applications, J. Memb. Sci. 523 (2017) 45–59. https://doi.org/10.1016/j.memsci.2016.09.058.

[31] S. Zhao, Z. Wang, J. Wang, S. Wang, The effect of pH of coagulation bath on tailoring the morphology and separation performance of polysulfone/polyaniline ultrafiltration membrane, J. Memb. Sci. 469 (2014) 316–325. https://doi.org/10.1016/j.memsci.2014.06.054.

[32] K. V. Kurada, S. De, Polyaniline doped ultrafiltration membranes: Mechanism of membrane formation and pH response characteristics, Polymer (Guildf). 153 (2018) 201–213. https://doi.org/10.1016/j.polymer.2018.08.032.

[33] I. Mav, M. Žigon, A. Šebenik, Sulfonated polyaniline, Synth. Met. 101 (1999) 717–718. https://doi.org/10.1016/S0379-6779(98)01166-7.

[34] S. Bhadra, N.H. Kim, J.H. Lee, Synthesis of water soluble sulfonated polyaniline and determination of crystal structure, J. Appl. Polym. Sci. 117 (2010) 2025–2035. https://doi.org/10.1002/app.32152.

[35] S.S. An, H.H. Yoon, G. Das, Amperometric urea biosensors based on sulfonated graphene/polyaniline nanocomposite, Int. J. Nanomedicine. (2015) 55. https://doi.org/10.2147/IJN.S88315.

[36] L. Li, S. Shahid, D. Alec, E. Anna, C. Emanuelsson, Flexible electro-responsive in-situ polymer acid doped polyaniline membranes for permeation enhancement and membrane fouling removal, 578 (2019) 263–272. https://doi.org/10.1016/j.memsci.2018.09.070.

[37] J. Jang, J. Ha, J. Cho, Fabrication of Water-Dispersible Polyaniline-Poly(4-styrenesulfonate) Nanoparticles For Inkjet-Printed Chemical-Sensor Applications, Adv. Mater. 19 (2007) 1772–1775. https://doi.org/10.1002/adma.200602127.

[38] B.T. McVerry, J.A.T. Temple, X. Huang, K.L. Marsh, E.M. V. Hoek, R.B. Kaner, Fabrication of Low-Fouling Ultrafiltration Membranes Using a Hydrophilic, Self-Doping Polyaniline Additive, Chem. Mater. 25 (2013) 3597–3602. https://doi.org/10.1021/cm401288r.

[39] C. Topacli, A. Topacli, Infrared spectra simulation for some sulfonamides by using semi-empirical methods, Spectrosc. Lett. 35 (2002) 207–217. https://doi.org/10.1081/SL-120003806.

[40] T. Sata, Ion exchange membranes and separation processes with chemical reactions, J. Appl. Electrochem. 21 (1991) 283–294. https://doi.org/10.1007/BF01020210.

[41] G. Chamoulaud, D. Bélanger, Chemical Modification of the Surface of a Sulfonated Membrane by Formation of a Sulfonamide Bond, Langmuir. 20 (2004) 4989–4995. https://doi.org/10.1021/la036285l.

[42] B.P. Tripathi, T. Chakrabarty, V.K. Shahi, Highly charged and stable cross-linked 4,4′-bis(4-aminophenoxy)biphenyl-3,3′-disulfonic acid (BAPBDS)-sulfonated poly(ether sulfone) polymer electrolyte membranes impervious to methanol, J. Mater. Chem. 20 (2010) 8036. https://doi.org/10.1039/c0jm01183e.

[43] P. Chapman, X.X. Loh, A.G. Livingston, K. Li, T.A.C. Oliveira, Polyaniline membranes for the dehydration of tetrahydrofuran by pervaporation, 309 (2008) 102–111. https://doi.org/10.1016/j.memsci.2007.10.016.

[44] Westerhof HP, Picken SJ, On the structure and dissolution properties of poly(p-phenylene terephthalamide) effect of solvent composition, Delft University of Technology, 2009.

[45] S. Bhadra, D. Khastgir, Determination of crystal structure of polyaniline and substituted polyanilines through powder X-ray diffraction analysis, Polym. Test. 27 (2008) 851–857. https://doi.org/10.1016/j.polymertesting.2008.07.002.

[46] S. Tan, A. Laforgue, D. Bélanger, Characterization of a Cation-Exchange/Polyaniline Composite Membrane, Langmuir. 19 (2003) 744–751. https://doi.org/10.1021/la0263054.

[47] P. Sivaraman, J.G. Chavan, A.P. Thakur, V.R. Hande, A.B. Samui, Electrochemical modification of cation exchange membrane with polyaniline for improvement in permselectivity, Electrochim. Acta. 52 (2007) 5046–5052. https://doi.org/10.1016/j.electacta.2007.02.016.

[48] Nidal Hilal; Ahmad Fauzi Ismail; Chris J Wright, Membrane Fabrication, CRC Press, 2015. https://doi.org/10.1201/b18149.

[49] P. Sukitpaneenit, T. Chung, Molecular elucidation of morphology and mechanical properties of PVDF hollow fiber membranes from aspects of phase inversion , crystallization and rheology,

340 (2009) 192–205. https://doi.org/10.1016/j.memsci.2009.05.029.

[50] D. Wang, K. Li, W.K. Teo, Porous PVDF asymmetric hollow fiber membranes prepared with the use of small molecular additives, 178 (2000) 13–23. https://doi.org/10.1016/S0376-7388(00)00460-9.

[51] J. Huang, R.B. Kaner, The intrinsic nanofibrillar morphology of polyaniline, (2006) 367–376. https://doi.org/10.1039/b510956f.

[52] M. Sadrzadeh, S. Bhattacharjee, Rational design of phase inversion membranes by tailoring thermodynamics and kinetics of casting solution using polymer additives, J. Memb. Sci. 441 (2013) 31–44. https://doi.org/10.1016/j.memsci.2013.04.009.

[53] C. Sun, Poly(vinylidene fluoride) membranes: Preparation, modification, characterization and applications, Chem. Eng. (2009) 193. https://doi.org/10.1016/j.actbio.2008.09.016.

[54] U. Rosenthal, J. Nechushtan, A. Kedem, D. Lancet, M.A. Frommer, An apparatus for studying the mechanism of membrane formation, Desalination. 9 (1971) 193–200. https://doi.org/10.1016/S0011-9164(00)80029-6.

[55] H. Strathmann, K. Kock, P. Amar, R.W. Baker, The formation mechanism of asymmetric membranes, Desalination. 16 (1975) 179–203. https://doi.org/10.1016/S0011-9164(00)82092-5.

[56] H.J. Kim, R.K. Tyagi, A.E. Fouda, K. Jonasson, The kinetic study for asymmetric membrane formation via phase-inversion process, J. Appl. Polym. Sci. 62 (1996) 621–629. https://doi.org/10.1002/(SICI)1097-4628(19961024)62:4<621::AID-APP5>3.0.CO;2-V.

[57] J.H. Kim, K.H. Lee, Effect of PEG additive on membrane formation by phase inversion, J. Memb. Sci. 138 (1998) 153–163. https://doi.org/10.1016/S0376-7388(97)00224-X.

[58] P.C. Rodrigues, G.P. De Souza, J.D. Da Motta Neto, L. Akcelrud, Thermal treatment and dynamic mechanical thermal properties of polyaniline, Polymer (Guildf). 43 (2002) 5493–

5499. https://doi.org/10.1016/S0032-3861(02)00401-9.

[59] E. Tarleton, J. Robinson, S. Smith, J. NA, New experimental measurements of solvent induced swelling in nanofiltration membranes, J. Memb. Sci. 261 (2005) 129–135. https://doi.org/10.1016/j.memsci.2005.02.037.

[60] A.F.M. Barton, Handbook of Solubility Parameters and Other Cohesion Parameters., CRC Press, 1983.

[61] L. Xu, S. Shahid, A.K. Holda, E.A.C. Emanuelsson, D.A. Patterson, Stimuli responsive conductive polyaniline membrane: In-filtration electrical tuneability of flux and MWCO, J. Memb. Sci. 552 (2018) 153–166. https://doi.org/10.1016/j.memsci.2018.01.070.

[62] M.J. Liu, K. Tzou, R.V. Gregory, Influence of the doping conditions on the surface energies of conducting polymers, Synth. Met. 63 (1994) 67–71. https://doi.org/10.1016/0379-6779(94)90251-8.

[63] M. Mänttäri, A. Pihlajamäki, M. Nyström, Effect of pH on hydrophilicity and charge and their effect on the filtration efficiency of NF membranes at different pH, J. Memb. Sci. 280 (2006) 311–320. https://doi.org/10.1016/j.memsci.2006.01.034.

[64] I.F.. Vankelecom, K. De Smet, L.E.. Gevers, A. Livingston, D. Nair, S. Aerts, S. Kuypers, P.A. Jacobs, Physico-chemical interpretation of the SRNF transport mechanism for solvents through dense silicone membranes, J. Memb. Sci. 231 (2004) 99–108. https://doi.org/10.1016/j.memsci.2003.11.007.

[65] L. Sun, H. Liu, R. Clark, S.C. Yang, Double-strand polyaniline, Synth. Met. 84 (1997) 67–68. https://doi.org/10.1016/s0379-6779(96)03839-8.

[66] M.A. Alaei Shahmirzadi, S.S. Hosseini, G. Ruan, N.R. Tan, Tailoring PES nanofiltration membranes through systematic investigations of prominent design, fabrication and operational parameters, RSC Adv. 5 (2015) 49080–49097. https://doi.org/10.1039/c5ra05985b.

[67] R.W. Baker, Membrane Technology and Applications, John Wiley & Sons, Ltd, Chichester, UK, 2004. https://doi.org/10.1002/0470020393.

[68] American Water Works Association, Microfiltration and Ultrafiltration Membranes for Drinking Water - Manual of Water Supply Practices, 2nd Editio, 2016.

[69] J. Shen, S. Shahid, I. Amura, A. Sarihan, M. Tian, Enhanced adsorption of cationic and anionic dyes from aqueous solutions by polyacid doped polyaniline, Synth. Met. 245 (2018) 151–159. https://doi.org/10.1016/j.synthmet.2018.08.015.

[70] 2001 Huang, L. & Nishinari, K., Interaction between poly(ethylene glycol) and water as studied by differential scanning calorimetry, J. Polym. Sci. 5 (2001) 496–50. https://doi.org/https://doi-org.ezproxy1.bath.ac.uk/10.1002/1099-0488(20010301)39:5<496::AID-POLB1023>3.0.CO;2-H.

[71] E. Sabadini, E.M. Assano, T.D.Z. Atvars, Molecular weight of polyethylene glycols by vapor pressure osmometry: An alternative data treatment, J. Appl. Polym. Sci. 65 (1997) 595–600. https://doi.org/10.1002/(SICI)1097-4628(19970718)65:3<595::AID-APP19>3.0.CO;2-W.

[72] L. Xu, S. Shahid, J. Shen, E.A.C. Emanuelsson, D.A. Patterson, A wide range and high resolution one-filtration molecular weight cut-off method for aqueous based nanofiltration and ultrafiltration membranes, J. Memb. Sci. 525 (2017) 304–311. https://doi.org/10.1016/j.memsci.2016.12.004.

[73] Y.H.S. Toh, X.X. Loh, K. Li, A. Bismarck, A.G. Livingston, In search of a standard method for the characterisation of organic solvent nanofiltration membranes, 291 (2007) 120–125. https://doi.org/10.1016/j.memsci.2006.12.053.

[74] N. Wang, J. Li, W. Lv, J. Feng, W. Yan, Synthesis of polyaniline/TiO2 composite with excellent adsorption performance on acid red G, RSC Adv. 5 (2015) 21132–21141. https://doi.org/10.1039/c4ra16910g.

[75] & B.E. Lunkwitz; Klaus, U., Buchammer; Heide-Marie, Permanent hydrophilic modification

of fluoropolymers, 1996.

[76] X. Yang, Experimental observations of nanofiltration with organic solvents, J. Memb. Sci. 190 (2001) 45–55. https://doi.org/10.1016/S0376-7388(01)00392-1.

[77] R. Levenstein, D. Hasson, R. Semiat, Utilization of the Donnan effect for improving electrolyte separation with nanofiltration membranes, J. Memb. Sci. 116 (1996) 77–92. https://doi.org/10.1016/0376-7388(96)00029-4.

Supporting Information to:

Simplified in-situ tailoring of cross-linked self-doped sulfonated polyaniline (S-PANI) membranes for nanofiltration applications

Hassan Alhweij[a,c,d], Emma Anna Carolina Emanuelsson[a,b], Salman Shahid[a,b,c*], Jannis Wenk[a,c*]
[a] Department of Chemical Engineering, University of Bath, Bath BA2 7AY, United Kingdom
[b] Centre for Advanced Separations Engineering, University of Bath, Bath BA2 7AY, United Kingdom
[c] Water Innovation and Research Centre (WIRC@Bath), University of Bath, Bath, BA2 7AY, United Kingdom
[d] Stantec UK Limited, Dominion House, Warrington, WA3 6GD, United Kingdom
* Corresponding authors
Jannis Wenk: j.h.wenk@bath.ac.uk
Salman Shahid: s.shahid@bath.ac.uk

Materials S1

Aniline, ammonium persulfate (APS), 4-methylpyridine (4MP), *N*-methyl-2-pyrrolidone (NMP), ammonium hydroxide solution, acetonitrile (ACN) HPLC grade, *N,N*-dimethylformamide (DMF), raffinose (MW 504.5 g mol^{-1}), sucrose octa-acetate (MW 678.6 g mol^{-1}), methylene blue (MW 319.8 g mol^{-1}), indigo carmine (MW 466.4 g mol^{-1}), bromothymol blue (MW 624.4 g mol^{-1}) and rose bengal (MW 1017.6 g mol^{-1}) were obtained from Sigma-Aldrich, UK. Methanol, 3-aminobenzene sulfonic acid (metanilic acid), sodium hydroxide and hydrochloric acid (HCl) aqueous solution were obtained from VWR, UK. Polyethylene glycol (PEG) 1000 g mol^{-1} was obtained from Fisher, UK. Commercial composite fluoropolymer flat sheet membrane (nominal MWCO 1000 g mol^{-1}) was obtained from Alfa Laval, UK.

S-PANI synthesis S2

S-PANI was synthesised by radical polymerisation of aniline and metanilic acid in the presence of ammonium persulfate in an acidic medium. During a typical synthesis, aniline was added to HCl solution (1.0 M). The mixture was then poured into a glass beaker surrounded by ice for cooling. Metanilic acid was added to the aniline-hydrochloric acid mixture and then stirred for 5 minutes using an overhead mechanical mixer fitted with a Teflon coated impeller. In a separate beaker, ammonium persulfate (APS) was dissolved in HCl solution (1.0 M). The APS-HCl solution was then added into the aniline flask drop by drop using a Watson Marlow peristaltic pump to allow control over the reaction temperature and formation of a reasonably long-chain polymer. The aniline, metanilic acid and APS were 1:1 molar ratio. The total APS-HCl solution addition period was around 13 h. After a reaction period of 24 h which involves APS addition and extended stirring, the solution was filtered (Whatman paper) and washed multiple times with pure water and then methanol until a neutral pH of the washing solution was reached. Subsequently, the powder was added to ammonium hydroxide solution (1.0 M) and left to mix using a magnetic stirrer for 1 h at room temperature to deprotonate the polymer salt to its base form. The powder was then washed down with pure water (1 L), followed by 200 mL of

methanol (50%, w/v) and finally 1 L of pure water. The filtered polymer powder was dried under a vacuum for 24 h at 60°C. The dry S-PANI powder was grounded by ceramic mortar and pestle, then passed through a 160 µm mesh sieve to remove any remaining clusters, leaving a fine powder with 72±1% yield based on the aniline monomer. This powder was then stored in plastic vials until required.

Fig. S1 shows the chemical structure of the formed S-PANI salt with the sulfonate functional group bonded with the aromatic benzene ring. The obtained powder was analysed by FT-IR to confirm that sulfonation had occurred.

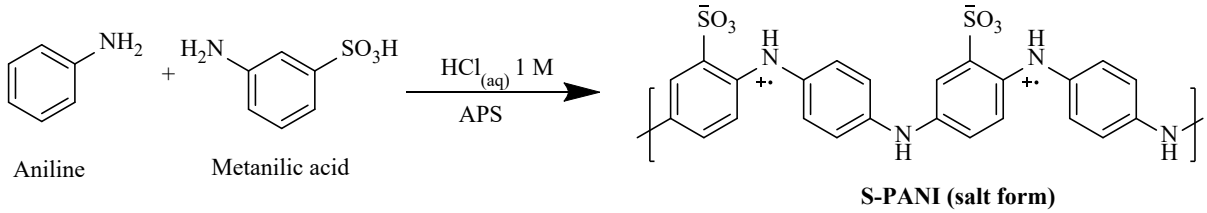

Fig. S1 Polymerisation scheme for S-PANI.

S-PANI molecular weight determination S3

All analysis was performed on an Agilent Infinity II MDS instrument equipped with differential refractive index (DRI), viscometry (VS), dual-angle light scatters (LS) and variable wavelength UV detectors. The system was equipped with 2 x PLgel Mixed D columns (300 x 7.5 mm) and a PLgel 5 µm guard column. The eluent is DMF with a 5 mmol NH_4BF_4 additive. Samples were solubilised overnight before filtration through a nylon membrane with 0.22 µm pore size before injection. Samples were run at 1 mL min^{-1} at 50°C. Poly(methyl methacrylate) standards (Agilent EasiVials) were used for calibration between 955,000–550 g mol^{-1}. Respectively, experimental molar mass (Mn, SEC) and dispersity (Đ) values of synthesized polymers were determined by conventional calibration using Agilent GPC/SEC software.

Energy dispersive X-ray S4

The element analysis of the S-PANI powder was studied via Scanning electron microscope- energy dispersive X-ray (SEM-EDX) using an FSEM (JSM-6301F, JEOL, Germany). The element analysis is shown in Table S1.

Table. S1 Element analysis (Atomic % and weight%) of S-PANI powder.

Element	Weight %	Atomic %
C	67.6±0.3	76.8±0.5
N	11.4±0.2	10.3±0.1
O	9.8±0.4	7.2±0.1
S	9.3±0.1	4.4±0.1
Cl	1.9±1.1	1.3±0.3

Membrane fabrication S5

For the cast film solution, S-PANI powder (20 wt%) was added in small portions to a mixture of NMP (74 wt%) and an anti-gelling agent 4MP (6 wt%). The mixture was stirred at 100 rpm for 2 h until a homogeneous solution was obtained and then left stirring at 50 rpm overnight. Afterwards, the polymer solution was left unstirred for 12 h for deaeration. A PET/PBT non-woven support layer (Novatexx 2484, 120 µm, Freudenberg Filter Technologies, Germany) was placed on a flat glass plate before casting. Elcometer 3540 film applicator was used to cast 200 µm membranes (clearance gap) at room temperature at a controlled relative humidity of ~30%. Membranes formed after immersion precipitation in the coagulation bath solution at room temperature, considering a consistent evaporation time of 10 seconds, before immersing the polymer solution into the coagulation bath. Different acidic strengths of coagulation solution (pure water, 1M HCl and 3M HCl) were used to produce membrane samples. After 24 h, some of the resulting membrane sheets were rinsed and stored at room temperature in pure water for a week, while the others were used freshly to understand the effect of H^+ ion leaching

on membrane morphology and transport properties. The rinsing water was changed daily to ensure complete H^+ ion removal from the membranes. A set of S-PANI membrane control samples was produced in a pure water coagulation bath and subsequently doped in acidic aqueous solutions (1M and 3M HCl) overnight to understand the effect of doping as a post-treatment of the membrane transport properties. The H^+ doped S-PANI membranes were rinsed with water for 5 min before use. In parallel, a set of the post-treated (doped) membranes was also rinsed in water for a week to assess the membrane performance after dedoping.

Membrane characterisation S6

FT-IR, XPS and XRD analysis

The chemical composition of S-PANI membranes was determined using an FT-IR spectrometer (PIKE Technologies Inc, USA) fitted with an attenuated total reflectance (ATR) accessory. Each FT-IR spectrum had 32 scans with 4 cm^{-1} resolution.

XPS data were acquired using a Kratos Axis SUPRA using monochromated Al kα (1486.69 eV) X-rays at 15 mA emission and 12 kV HT (180W) and a spot size/analysis area of 700 x 300 µm. The instrument was calibrated to gold metal Au 4f (83.95 eV) and dispersion adjusted to give a binding energy (BE) of 932.6 eV for the Cu 2p3/2 line of metallic copper. Ag 3d5/2 line FWHM at 10 eV pass energy was 0.544 eV. Source resolution for monochromatic Al Kα X-rays is ~0.3 eV. The instrumental resolution was determined to be 0.29 eV at 10 eV pass energy using the Fermi edge of the valence band for metallic silver. Resolution with charge compensation system on <1.33 eV FWHM on PTFE. High-resolution spectra were obtained using a pass energy of 20 eV, step size of 0.1 eV and sweep time of 60 seconds, resulting in a line width of 0.696 eV for Au 4f7/2. Survey spectra were obtained using a pass energy of 160 eV. Charge neutralisation was achieved using an electron flood gun with filament current = 0.38 A, charge balance = 2 V, filament bias = 4.2 V. Successful neutralisation was adjudged by analysing the C 1s region wherein a sharp peak with no lower BE structure was obtained. Spectra have been charge corrected to the mainline of the carbon 1s spectrum (adventitious carbon) set to 284.8 eV. All data was

recorded at a base pressure of below 9 x 10-9 Torr and a room temperature of 294 K. Data was analysed using CasaXPS v2.3.19PR1.0. Peaks were fit with a Shirley background before component analysis.

X-ray diffractometry (XRD) was used to characterise M1, M2 and M3. XRD spectra were scanned on a STOE STADI P double setup, equipped with mythen detectors, using pure Cu-Kα1 radiation (λ= 1.54060 Å).

Ion exchange capacity (IEC), Water uptake (WU), hydrolytic and alkalinity stability

After immersion in pure water for one day, membrane samples were subsequently immersed for one day in 100 mL of HCl(aq) solution to fully protonate the polymeric structure. The membrane was then washed and equilibrated for 4 h with distilled water, while the distilled was changed several times to remove the last traces of acid. The membrane was then equilibrated with 50 ml of 0.01 M NaOH(aq) solution for 24 h and the cation exchange capacity was determined from the reduction in alkalinity determined by back titration. The ion exchange capacity of the cation exchange membrane was calculated using equation:

$$IEC = \frac{V_{NaOH}\ x\ S_{NaOH}}{m_{dry}} \quad (1)$$

where, V_{NaOH} is the volume of NaOH used in the titration, m_{dry} is the dry weight of the membrane in g, and S_{NaOH} is the strength of NaOH used for the determination of IEC (meq g^{-1}).

Water uptake was measured by first drying all membranes at 40°C for 24 h and the dry mass of individual membrane strips was recorded. The membrane strips were then immersed individually in pure water at room temperature for 24 h. The water remaining on the surface of the wetted membrane was carefully dried utilizing absorbent paper before weighing. The water uptake was calculated as:

$$WU = \left(\frac{m_{wet} - m_{dry}}{m_{dry}}\right) \times 100 \quad (2)$$

Where m_{wet} is the mass of the swollen membrane after equilibrium and m_{dry} is the mass of the dry membrane.

The hydrolytic stability test of the membranes was explored by weighing the dried samples before and after wetting at different water bath temperatures 20, 40, 80°C for 4 h. UV spectroscopy was also used to look for small changes in the absorption of the solution.

The S-PANI membranes M1-M3 were cut into strips with approximate dimensions of 75 x 5.5 mm. The samples were dried in a vacuum oven overnight and then the dimensions of the dried samples were measured. Afterwards, the membranes were soaked in pure water at 20, 40 and 80°C overnight. Afterwards, the samples were dried in a vacuum oven and the final dimensions were measured.

The membrane stability in alkaline solution was tested by weighing the dried samples before and after wetting in the alkaline solution (0.1 NaOH(aq)) at 20°C for 24 h.

Morphology and porosity

The morphological properties of the membranes were investigated by SEM (SU3900, Hitachi, Japan). To analyse membrane morphology, SEM images on both the surface and the cross-section of membranes were captured at an acceleration voltage of 10 kV. A representative cross-section was obtained by fracturing membranes in liquid nitrogen. Samples were mounted onto SEM stubs and coated with gold using a sputter coater (S150B, Edwards, USA). Change of skin layer thickness was determined for different coagulation bath conditions.

Also, the re-assembly (precipitation) process of S-PANI polymer solution in neutral and acid aqueous solution was investigated by dissolving 0.2 wt% of S-PANI powder into NMP and adding 2 mL of the solution to either 18 mL of pure water, 1 M and 3 M HCl, respectively. The precipitated polymer was dipped into a copper grid and submitted to transmission electron microscopy (TEM), JEOL JSM-2100Plus .

Adsorption isotherms, combined with the Brunauer-Emmet-Teller (BET) theory for multilayer adsorption, allowed the determination of the internal surface area of the membrane. Although the use of gas adsorption isotherm is more common for characterisation of porous media, its application in membrane research was reported elsewhere [1]. The application of this method was seen as complementary to other methods due to the low membrane porosities as well as difficulties in correctly interpreting these results [2]. N_2 adsorption-desorption measurements were performed with a

Micromeritics; model 3 Flex 3500, USA. For porosity measurements, separate batches of M1-M3 were prepared without a support layer. Membrane samples were first dried at ambient laboratory conditions. Afterwards, each sample was placed in a sample tube to ensure complete drying and degassing at 40°C for 24 h. The specific surface area and pore size distribution measurements were completed within 24 h in a liquid nitrogen bath.

Demixing kinetics

Polymer films along with the glass plate were immersed in coagulation solution to produce membranes M1 to M3. Samples of the coagulation solution were taken at hourly intervals over 8 h and after 24 h at 6 mm distance to the cast film. Change of organic (solvent) concentration was measured using a total organic carbon analyser (TOC-L CPH, Shimadzu, Japan). The demixing rate was determined by plotting the change of relative concentration of TOC in the coagulation solution at time (t) and at infinite time (∞) defined here as 24 h immersion.

Thermal and mechanical analysis

The thermal degradation property of the S-PANI was studied by thermogravimetric analysis (TGA, TA instruments Q-500). All S-PANI membrane samples were heated from 30 to 600°C with an airflow rate of 60 mL min^{-1} and a heating rate of 10°C min^{-1}. Differential scanning calorimeter (DSC, TA Instruments Q2000) measurements were implemented under a nitrogen flow rate of approximately 20 mL min^{-1} at a heating rate of 10°C min^{-1} from 30 to 300°C.

Tensile strength and % elongation at breakage of the S-PANI membranes were measured to assess the effect of the cross-linking on the membranes' mechanical properties. An Instron 3369 mechanical tester was used and dried membrane casts without a support layer were cut into rectangular strips of approximately 70 mm × 6 mm for testing. All tests were conducted with a pull speed of 2 mm min^{-1} at room temperature. The membrane thickness was measured using standard Vernier callipers. The reported mechanical data is an average of three different membrane samples.

Solvent stability

Solvent stability of M1-M3 was determined by immersion for two weeks in DMA solvent. To understand the role of sulfonic groups in the cross-linking process, PANI powder was prepared following the protocol described in section S-PANI synthesis S2 but without metanilic acid. Afterwards, PANI membranes were prepared while mimicking the coagulation bath conditions as used for M1-M3. The obtained PANI membranes were also immersed in DMA for two weeks and labelled as M1'-M3'.

Mass swelling degree and gel content

A set of organic solvents such as Methanol (MeOH), Isopropanol (IPA), Acetone (AC), Toluene (TOL), Tetrahydrofuran (THF) were used to determine the membrane swelling and stability. In terms of polarity, MeOH and IPA are polar protic solvents, AC and THF are polar aprotic solvents, and TOL is a nonpolar solvent. M1-M3 were cut into small samples (2 cm × 2 cm) and dried in the vacuum oven. The dried membrane samples (of known mass) were allowed to equilibrate with an excess of the solvent in a sealed flask at 25°C for 1 h. The swollen membranes were taken from the solvent and quickly dried with filter paper to remove solvent from the external surface. The mass of the swollen membranes was then determined. The mass swelling degree (SD) was calculated using the following equation:

$$SD = \left(m_{wet} - m_{dry}\right)/m_{dry} \quad (3)$$

where m_{wet} is the mass of the swollen membrane after equilibrium and m_{dry} is the mass of the dry membrane.

The stability of the S-PANI membranes in the solvents was determined by immersing the membrane sample in the solvent for two weeks (same conditions as per swelling test) including for DMF. After two weeks, the membrane samples were removed from the solvent and dried in the vacuum oven. The mass change of the dry membrane before and after soaking in the solvent indicates membrane dissolution. The gel content is a parameter that is used to define the polymer stability in different solvent was calculated by using the following equation:

$$Gel\ content\ \% = (W_a/W_b)\ x\ 100 \quad (4)$$

where W_b and W_a is the dry weight of the membrane sample before and after solvent soaking, respectively. Partially or fully dissolved membranes are designated as dissolved (for DMF). Moderately

swollen membranes or those with gel content below 90% are designated as swollen. Membranes that showed no swelling or dissolution in DMF and had a gel content higher than 90%, are designated crosslinked [3].

Contact Angle

The hydrophilicity of the membranes was measured (3 times per sample) by sessile dynamic droplet penetration using a contact angle goniometer (Contact Angle System OCA 15Pro, Dataphysics, Germany). A small droplet of water (2.0 µL) was placed onto the membrane surface at a dosing rate of 1.0 µL s^{-1} using a Hamilton syringe. The software SCA20 was used to calculate the dynamic effective contact angle (CA).

Membrane transport properties

Membrane filtration experiments were conducted in dead-end mode using a stainless steel chemically resistant dead-end cell (Sterlitech HP4750) with an active membrane area of 14.6 cm^2. The schematic of the experimental set-up is illustrated in Fig. S2. Permeate flow rates were measured using a digital scale connected to a computer. The software programme Labview 2011 was used to calculate the membrane permeance J_p(L m^{-2} hr^{-1} bar^{-1}) by using the following equation:

$$J_p = \frac{\Delta W}{A.\Delta P.t.\rho_p} \quad (5)$$

Where ΔW (kg) is the obtained permeate weight during a fixed time slot, ρ_s (kg m^{-3}) is the permeate density at room temperature, A (m^2) is the membrane coupon active surface area (filtration area), t is the time intervals between each measurement and ΔP (bar) represents the differential pressure at the membrane, which is maintained by the inline N_2 cylinder. For M1-M5 stability and performance changes related to the membrane, doping was assessed via pH measurements of permeates at different filtration stages, reported as an average of three membrane samples.

To define the effect on the membranes' solutes' retention, different batches of dye feed solutions ranging from 320 to 1017 g mol^{-1} were used sequentially. Methylene blue, indigo carmine, bromothymol blue and rose bengal dye powder were separately dissolved in pure water. For a typical dye solution, 10 mg

of dye powder was added to 1 L of pure water at room temperature except for bromothymol blue where 50 mg were added instead. The dye powder was dissolved and stirred using a magnetic stirrer at 200 rpm until the dye powder was completely dissolved.

Dye rejection was measured by filtering 50 mL of the fresh dye feed solution using a dead-end cell set-up. The dye concentration in the feed and permeate samples were measured via UV absorbance using an Agilent Carry 100 UV-Vis spectrometer (Agilent Corporation). For calibrations curves see Fig. S3-S6. The adsorbed dye mass on the membrane surface was quantified by conducting a mass balance for the M1 membrane sample. The dye rejection was calculated using the following equation:

$$R\% = \left(1 - \frac{C_p}{C_f}\right) \times 100 \quad (6)$$

Where C_p is the dye solution concentration in the permeate and C_f is that in the feed.

The membrane surface charge and the dye feed solutions were measured (3 times per sample) to understand the charge interactions between the membranes and the dye solutes. The surface charge of M1-M5 and M8 was measured by using Zetasizer nano series model ZS, Malvern-Panalytical, UK. Zeta potential planar cell (ZEN 1020) along with tracer particles (Latex beads, polystyrene 0.3 μm mean particle size) were used to measure the electrophoretic mobility of the particles at varying distances from the planar surface at neutral pH. The zeta potential of the dye solution feed was measured with a Zetasizer (Malvern-Panalytical Instruments, UK) at 20°C.

The MWCO of membranes, defined as the MW weight at 90% solute retention [4], was obtained using the 90% retention value for rejection curves recorded with PEG and two sugars of a defined MW, as described in detail in SI, Materials S1.

To prepare PEG feed solution, 600 mg of PEG 1000 g mol^{-1} was added to 1 L of pure water and continuously stirred at 200 rpm until complete dissolution. The PEG feed solution (50 mL) was filtered through the dead-end cell to obtain 25 mL permeate. The PEG concentrations were analysed by an Agilent 1260 infinity series high-performance liquid chromatography (HPLC) machine equipped with an evaporative light scattering (ELSD) detector. A flow rate of 1.0 mL min^{-1} was used with mobile phase acetonitrile/water (15/85). Analytic peaks were analysed using an established method for MWCO determination by using 1000 g mol^{-1} PEG exclusively [5]. Calibration curves are provided in Fig S7-

S14. Raffinose and sucrose octa-acetate aqueous solutions (20 mg L^{-1} as TOC) were also used to verify the MWCO of the obtained NF membrane.

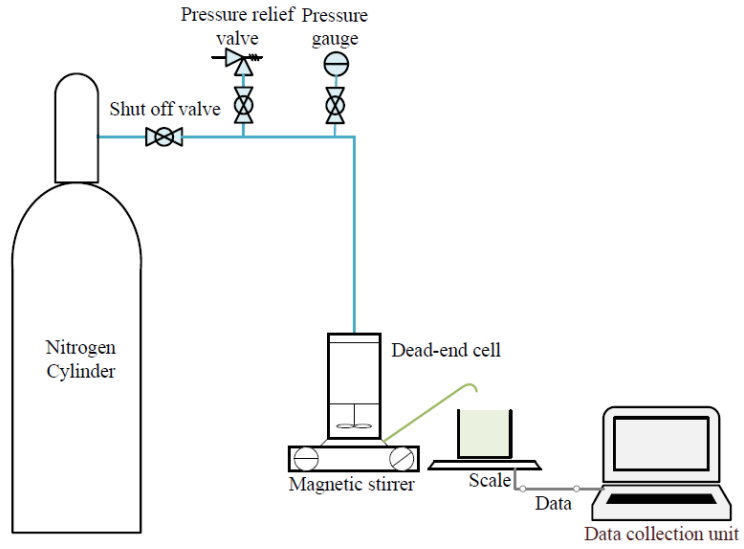

Fig. S2 Schematic diagram of the dead-end cell filtration.

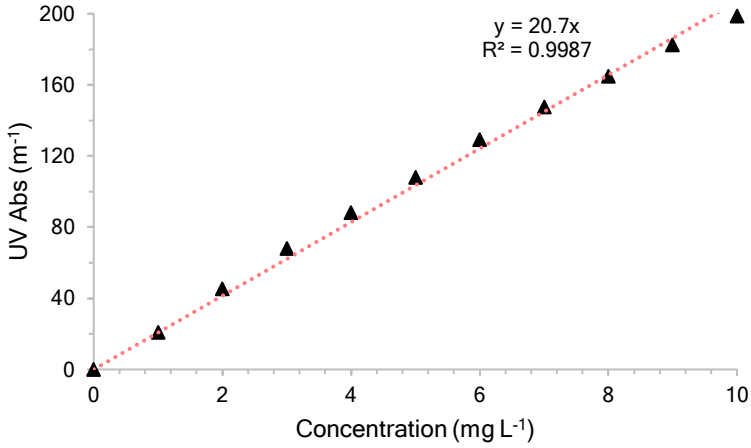

Fig. S3 The calibration curve of methylene blue dye aqueous solution as a relation between the feed solution concentration and the UV absorbance (peak absorption at wavelength 661 nm).

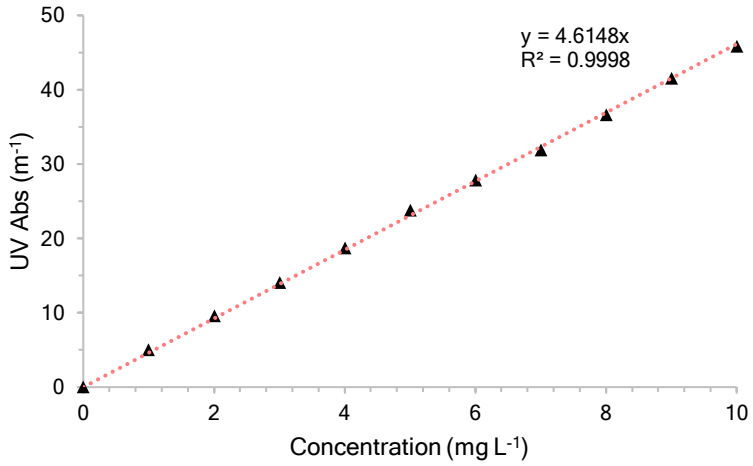

Fig. S4 The calibration curve of indigo carmine dye aqueous solution as a relation between the feed solution concentration and the UV absorbance (peak absorption at wavelength 612 nm).

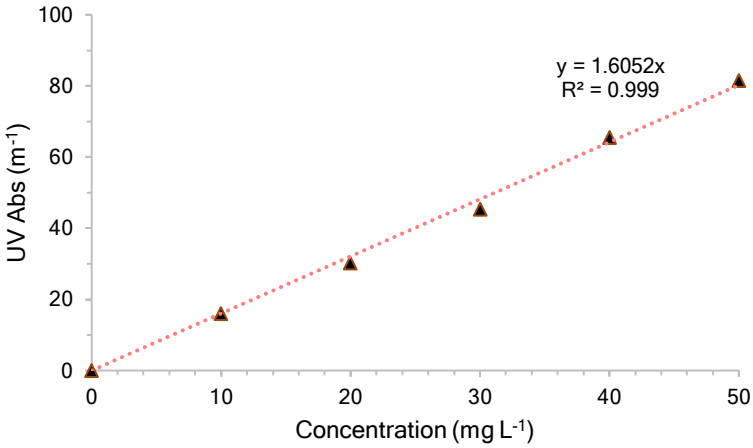

Fig. S5 The calibration curve of bromothymol blue dye aqueous solution as a relation between the feed solution concentration and the UV absorbance (peak absorption at wavelength 430 nm).

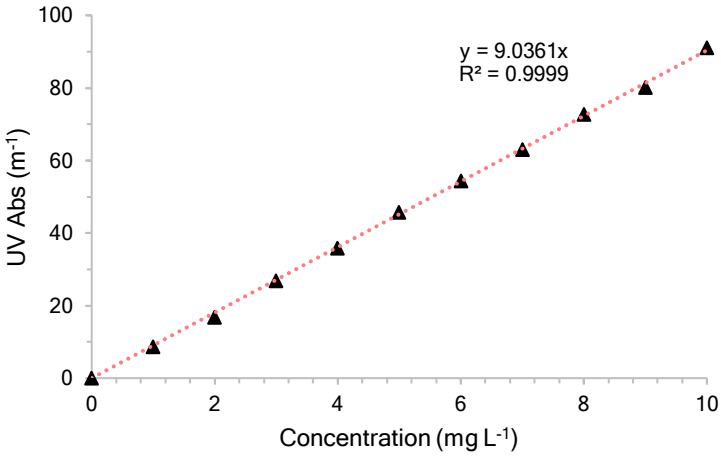

Fig. S6 The calibration curve of rose bengal dye aqueous solution as a relation between the feed solution concentration and the UV absorbance (peak absorption at wavelength 549 nm).

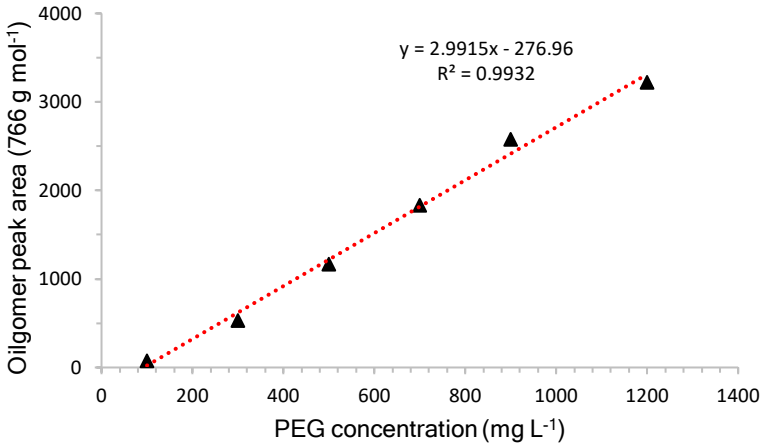

Fig. S7 The calibration curve of the PEG oligomer MW 766 g mol^{-1} at different concentrations.

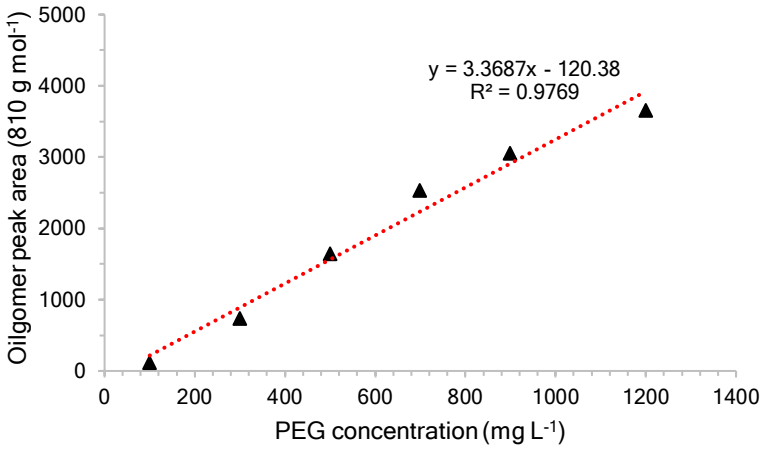

Fig. S8 The calibration curve of the PEG oligomer MW 810 g mol^{-1} at different concentrations.

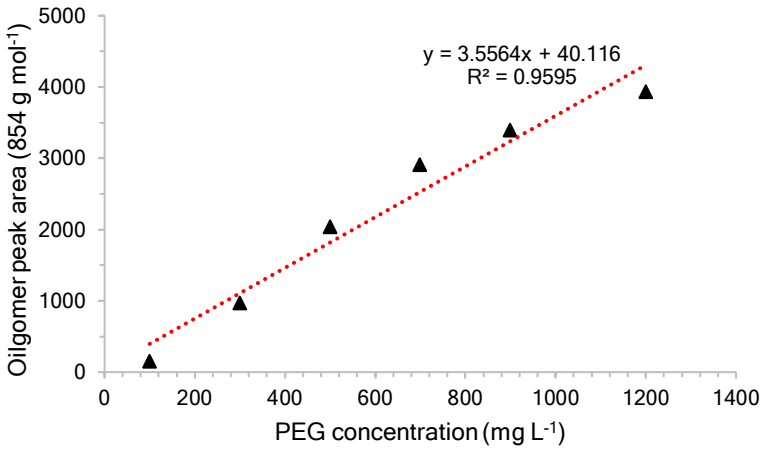

Fig. S9 The calibration curve of the PEG oligomer MW 854 g mol^{-1} at different concentrations.

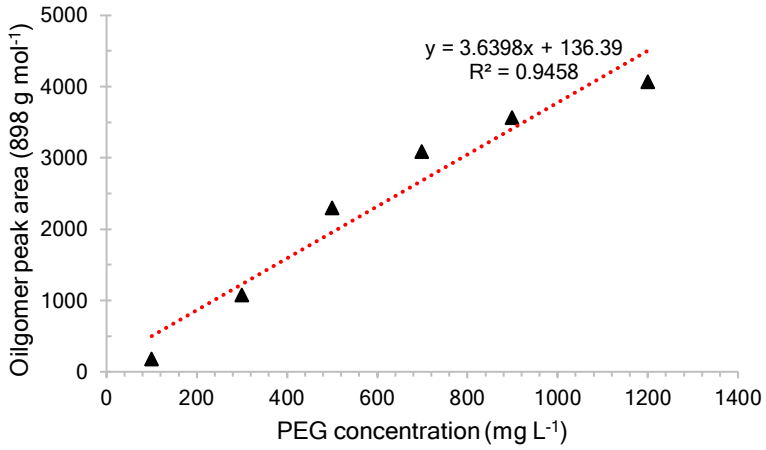

Fig. S10 The calibration curve of the PEG oligomer MW 898 g mol^{-1} at different concentrations.

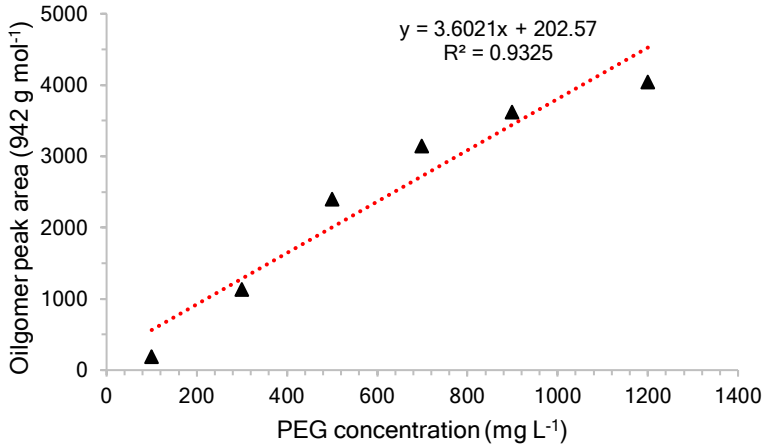

Fig. S11 The calibration curve of the PEG oligomer MW 942 g mol^{-1} at different concentrations.

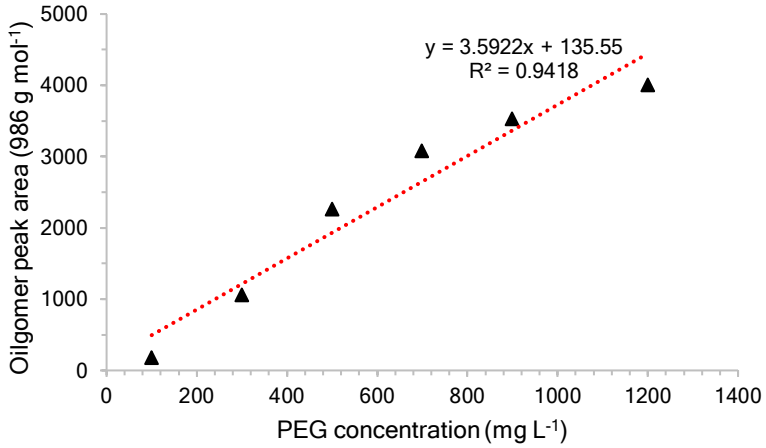

Fig. S12 The calibration curve of the PEG oligomer MW 986 g mol^{-1} at different concentrations.

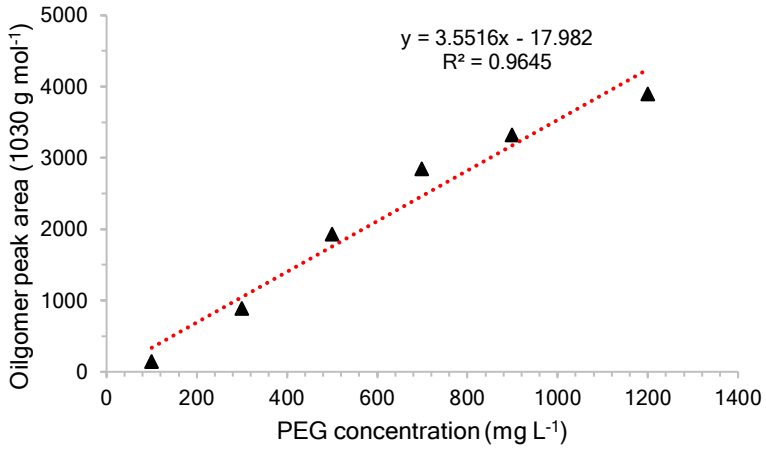

Fig. S13 The calibration curve of the PEG oligomer MW 1030 g mol^{-1} at different concentrations.

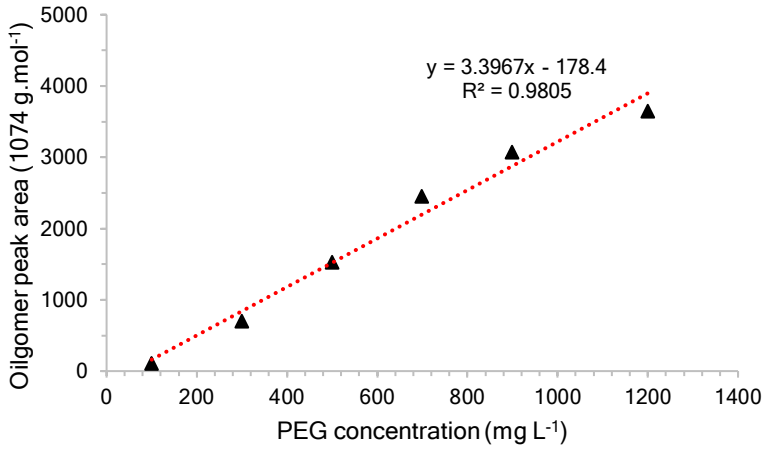

Fig. S14 The calibration curve of the PEG oligomer MW 1074 g mol^{-1} at different concentrations.

S-PANI doping S7

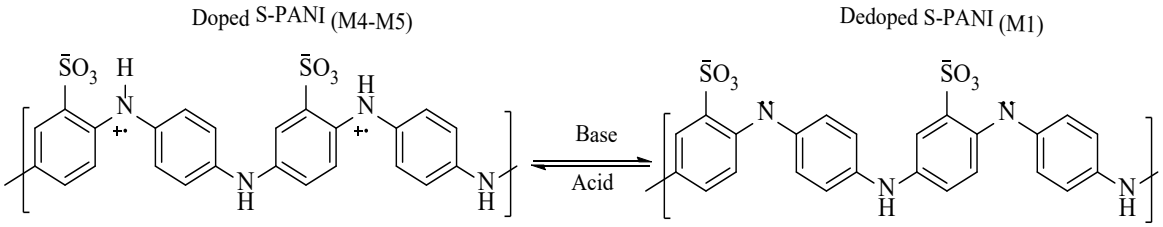

Fig. S15 pictorial representation of both doped/dedoped M4-M5 and M1 membranes.

XPS spectra S8

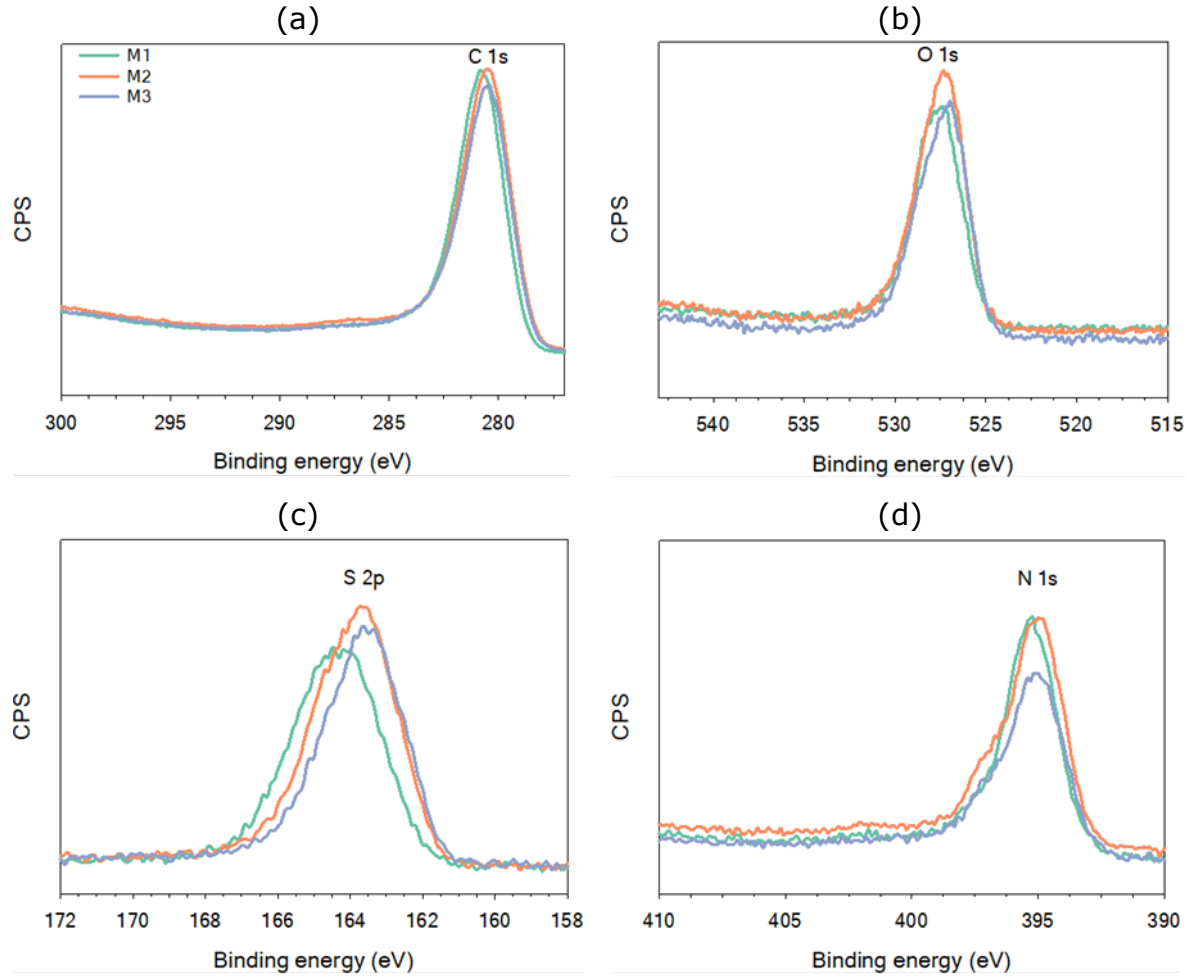

Fig. S16 Core-level spectra of S-PANI membranes M1-M3 (a) C 1s (b) O 1s (c) S 2p (d) N 1s.

Water stability S9

Table. S2 Hydrolytic and alkalinity stability of S-PANI membranes M1-M3.

Membrane	Weight loss in DI water (%)			Weight loss in 0.1 NaOH(aq)
	20°C	40°C	80°C	20°C
M1	None	None	None	None
M2	None	None	None	None

M3	None	None	None	None

Morphology S10

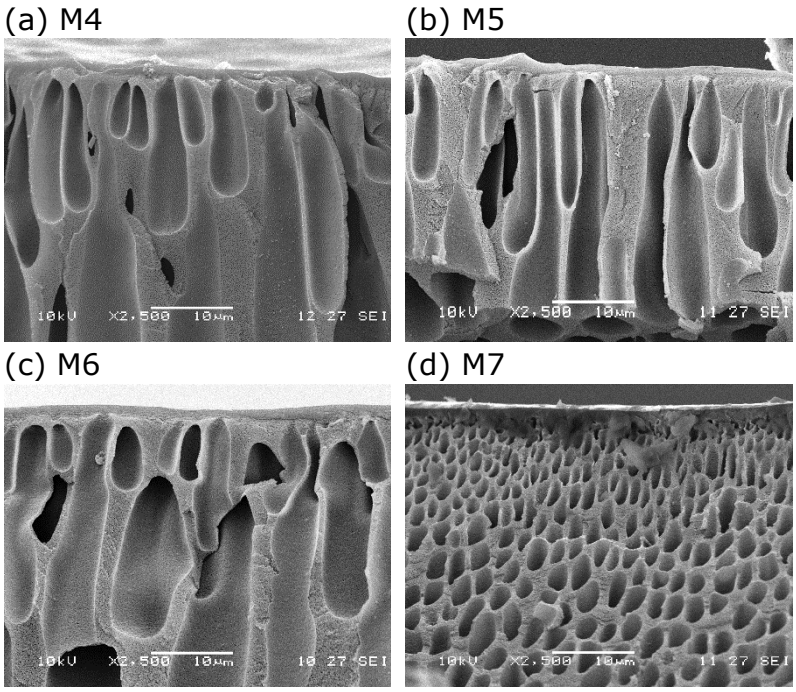

Fig. S17. SEM surface and cross-sectional area images of HCl doped S-PANI membranes prepared in neutral coagulation bath (M4-M5), 1M HCl acidic coagulation bath (M6) and 3M HCl acidic coagulation bath (M7).

Porosity S11

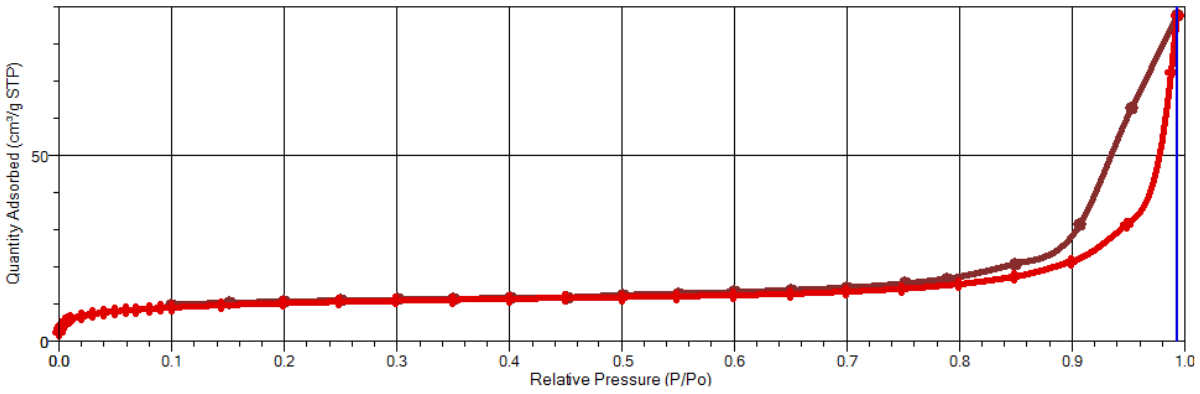

Fig. S18 The isotherm of the S-PANI membrane produced in pure water coagulation bath (M1).

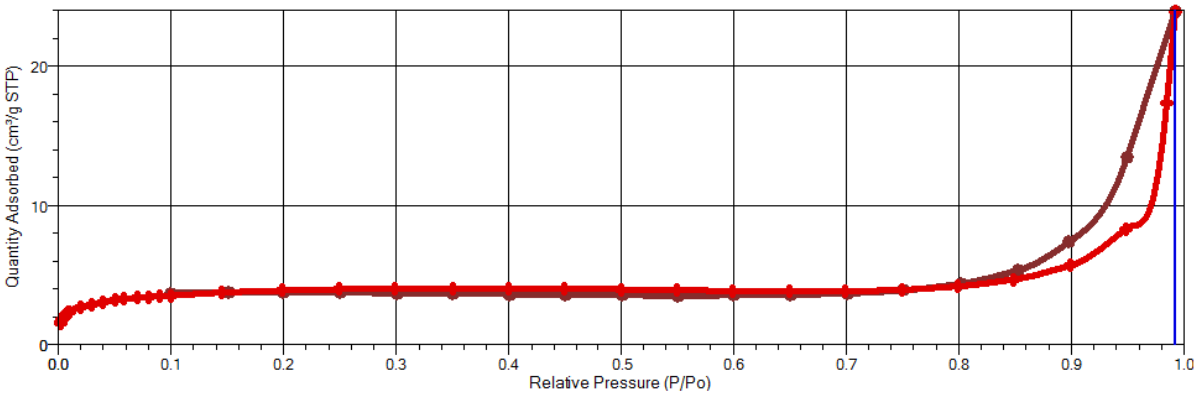

Fig. S19 The isotherm of the S-PANI membrane produced in 1M HCl(aq) coagulation bath (M2).

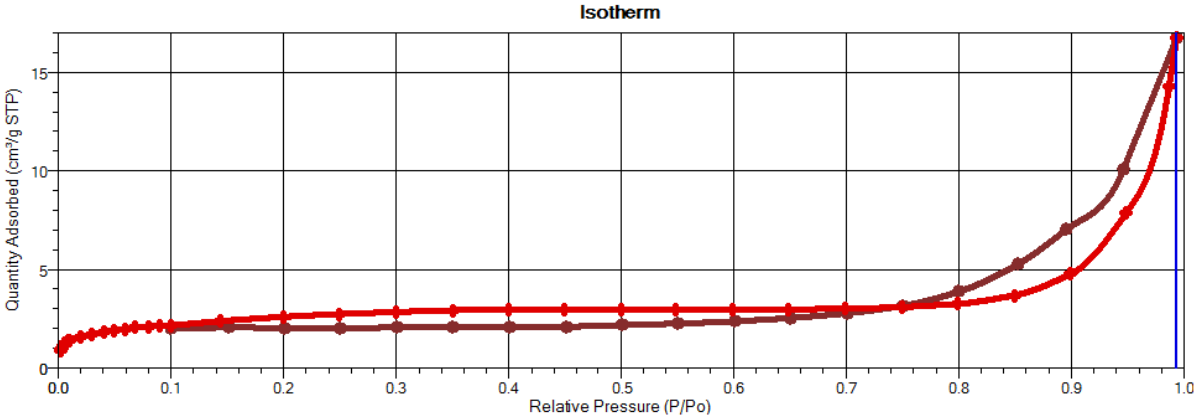

Fig. S20 The isotherm of the S-PANI membrane produced in 3M HCl(aq) coagulation bath (M3).

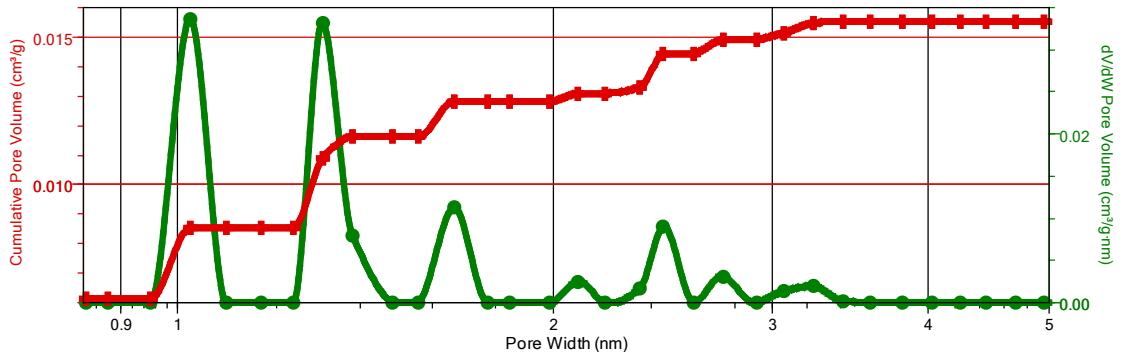

Fig. S21 The cumulative pore volume versus the pore width of the S-PANI membranes prepared in a neutral coagulation bath (M1) without a support layer.

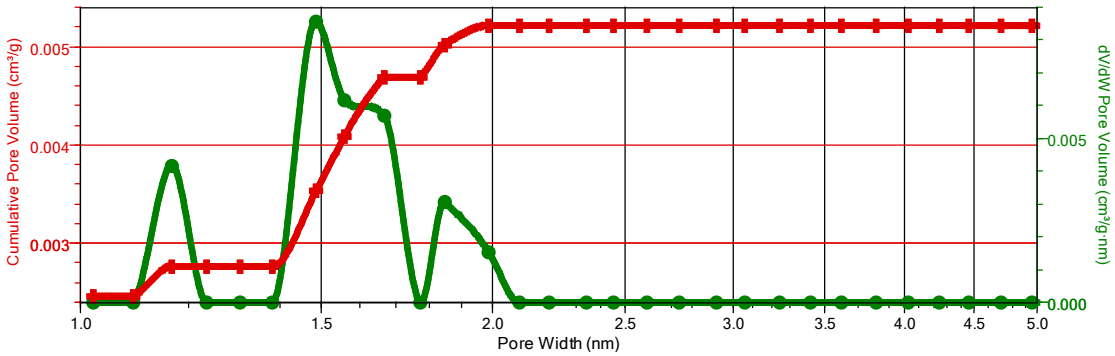

Fig. S22 The cumulative pore volume versus the pore width of the S-PANI membranes prepared in 1M HCl acidic coagulation bath (M2) without a support layer.

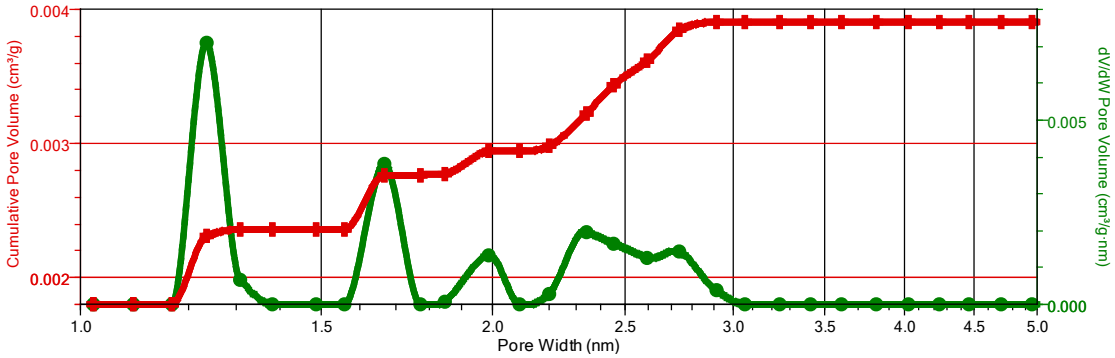

Fig. S23 The cumulative pore volume versus the pore width of the S-PANI membranes prepared in 3M HCl acidic coagulation bath (M3) without a support layer.

Differential scanning calorimetry S12

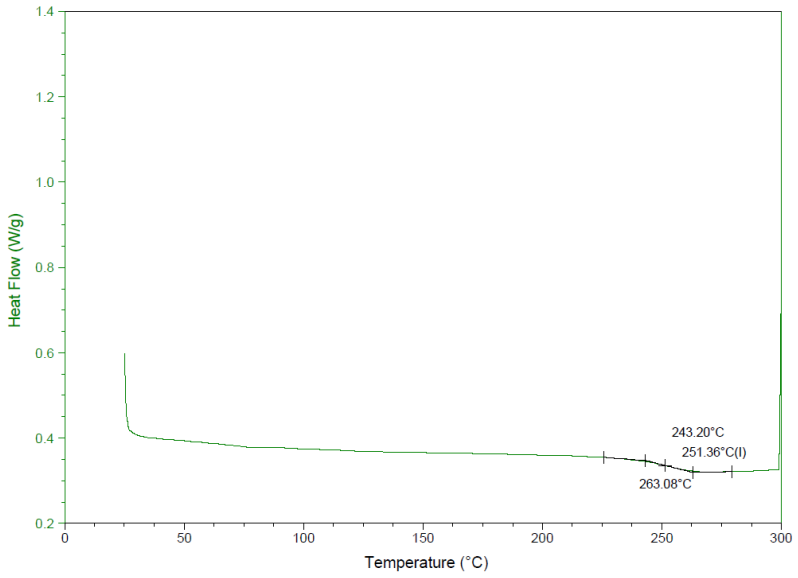

Fig. S24 DSC thermogram register from 20 to 300°C of M1 S-PANI membrane produced in DI water coagulation bath.

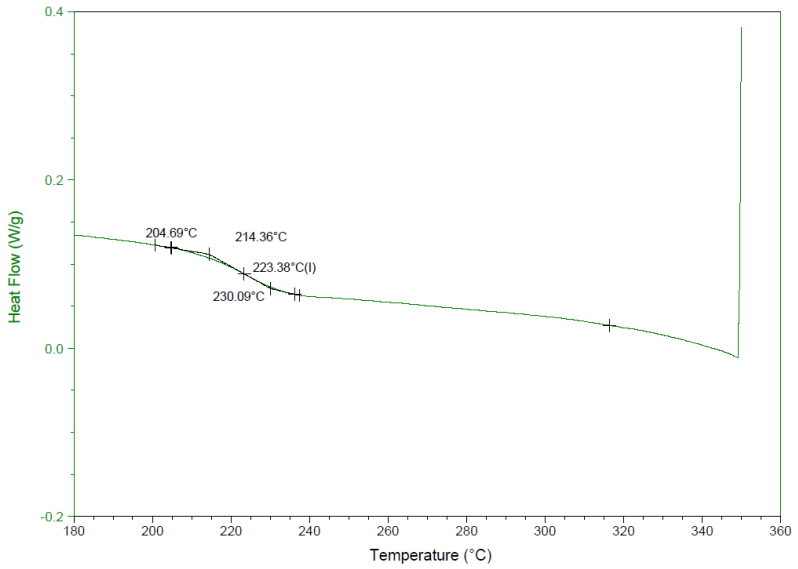

Fig. S25 DSC thermogram register from 150 to 350°C of M1 S-PANI membrane produced in 1M HCl coagulation bath.

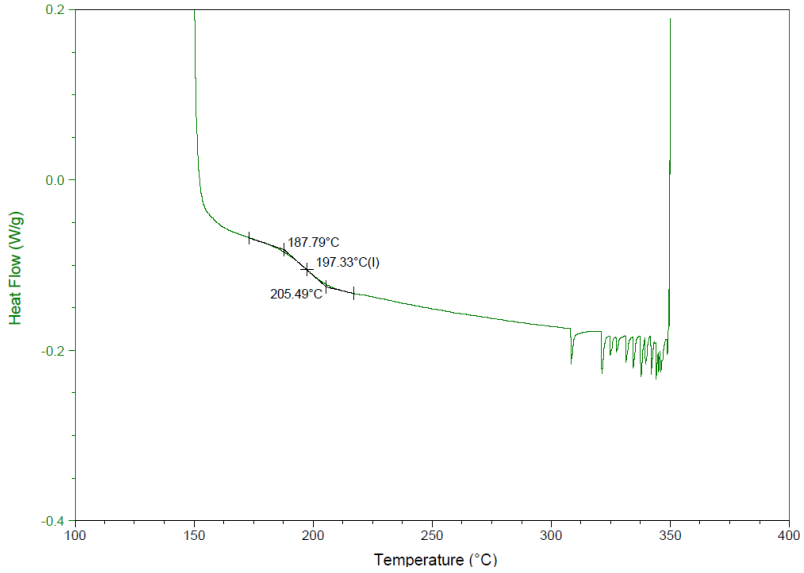

Fig. S26 DSC thermogram register from 150 to 350°C of M1 S-PANI membrane produced in 3M HCl coagulation bath.

Transport properties S13

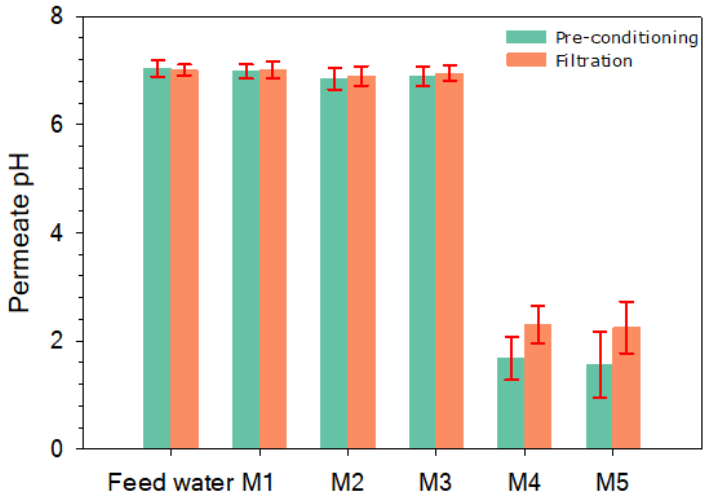

Fig. S27 pH change of the M1-M5 membranes' permeate after preconditioning and filtration.

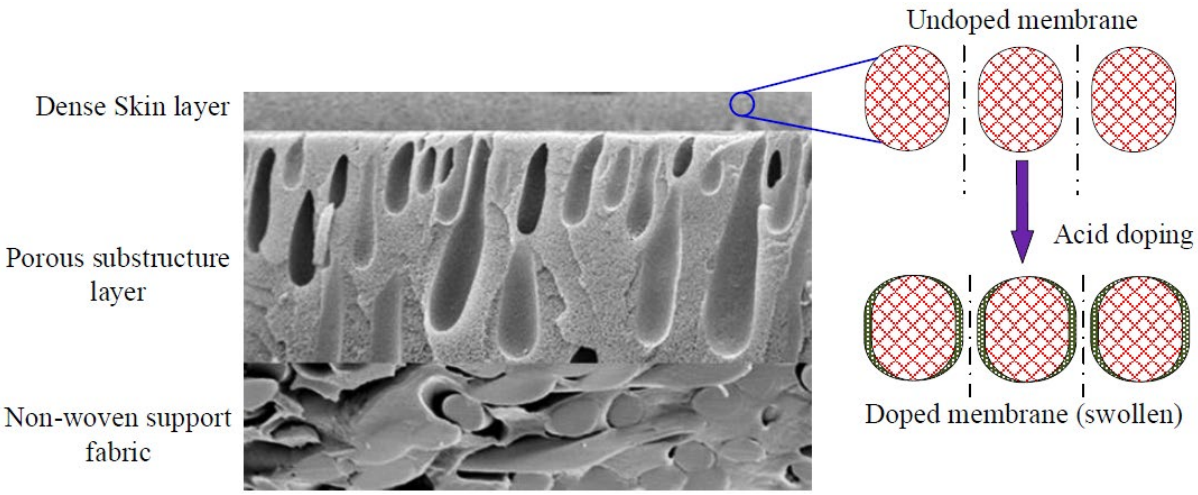

Fig. S28 A schematic representation of asymmetric S-PANI membrane and matrix swelling and pore contraction of the membrane after HCl(aq) acid doping.

Table. S3 The dye removal mechanism of the S-PANI M1 membrane.

Dye	MW (g mol^{-1})	Total rejection (%)	Size exclusion (%)	Adsorption (%)
Rose bengal	1017.6	84±6.9	74±0.1	26±0.1
Indigo carmine	466.4	73±0.1	58±0.5	42±0.5
Methylene blue	319.8	50±3	84±0.2	16±0.2

References

[1] T. Virtanen, G. Rudolph, A. Lopatina, B. Al-Rudainy, H. Schagerlöf, L. Puro, M. Kallioinen, F. Lipnizki, Analysis of membrane fouling by Brunauer-Emmet-Teller nitrogen adsorption/desorption technique, Sci. Rep. 10 (2020) 3427. doi:10.1038/s41598-020-59994-1.

[2] J.I. Calvo, P. Prádanos, A. Hernández, W.R. Bowen, N. Hilal, R.W. Lovitt, P.M. Williams, Bulk and surface characterization of composite UF membranes Atomic force microscopy, gas adsorption-desorption and liquid displacement techniques, J. Memb. Sci. 128 (1997) 7–21. doi:10.1016/S0376-7388(96)00304-3.

[3] K. Vanherck, A. Cano-Odena, G. Koeckelberghs, T. Dedroog, I. Vankelecom, A simplified diamine crosslinking method for PI nanofiltration membranes, J. Memb. Sci. 353 (2010) 135–143. doi:10.1016/j.memsci.2010.02.046.

[4] D.A. Rohani, Rosiah, Hyland, Margaret & Patterson, A Refined One-Filtration Method for Aqueous Based Nanofiltration and UltraFiltration Membrane Molecular Weight Cut-Off Determination using Polyethylene Glycols, 382 (2011) 278–290. doi:https://doi.org/10.1016/j.memsci.2011.08.023.

[5] L. Xu, S. Shahid, J. Shen, E.A.C. Emanuelsson, D.A. Patterson, A wide range and high resolution one-filtration molecular weight cut-off method for aqueous based nanofiltration and ultrafiltration membranes, J. Memb. Sci. 525 (2017) 304–311. doi:10.1016/j.memsci.2016.12.004.